Particulate matter sources and the impact of Cyclone Gabrielle on the Hastings airshed

Prepared for: Hawke's Bay Regional Council January 2025

Hawkes Bay Regional Council Publication No. 5679

HAWKES BAY
REGIONAL COUNCIL
TE KAUNIHERA Ā-ROHE O TE MATAU-A-MĀUI

ISSN 2703-2051 (Online)
ISSN 2703-2043 (Print)

HAWKES BAY REGIONAL COUNCIL
TE KAUNIHERA Ā-ROHE O TE MATAU-A-MĀUI

(06) 835 9200
0800 108 838
Private Bag 6006 Napier 4142
159 Dalton Street . Napier 4110

Environmental Science

Particulate matter sources and the impact of Cyclone Gabrielle on the Hastings airshed

Prepared for: Hawke's Bay Regional Council January 2025

Hawkes Bay Regional Council Publication No. Report number 5679

Reviewed By:
Jeremy Kidd – Air Quality Scientist

Approved By:
Dr Haley Ataera – Science Manager

ISSN 2703-2051 (Online)
ISSN 2703-2043 (Print)

.

Particulate matter sources and the impact of Cyclone Gabrielle on the Hastings airshed

PK Davy WJ Trompetter

GNS Science Consultancy Report 2024/99
January 2025

DISCLAIMER

Use of Data:

Date that GNS Science can use associated data: February 2025

BIBLIOGRAPHIC REFERENCE

Davy PK, Trompetter WJ. 2025. Particulate matter sources and the impact of Cyclone Gabrielle on the Hastings airshed. Lower Hutt (NZ): GNS Science. 63 p. Consultancy Report 2024/99.

CONTENTS

FIGURES

TABLES

APPENDICES

APPENDIX FIGURES

APPENDIX TABLES

EXECUTIVE SUMMARY

This report presents the results of an analysis of particulate-matter concentrations and composition from a $PM_{2.5}$ and $PM_{10–2.5}$ sampling campaign at Hastings in the Hawke's Bay. Particulate-matter samples were collected from May 2023 to August 2024, which included two winter periods. The compositional data have been used in a receptor modelling study to apportion particulate-matter emission sources contributing to ambient particulate-matter concentrations in Hastings. Understanding the sources of fine-particle air pollution is important for air-quality management and the prevention of health impacts for exposed populations.

The work also served to examine the relative impact on sources of particulate matter in the Hastings airshed after the flooding and subsequent silt deposition caused by Cyclone Gabrielle.

Five main source types were extracted from the data by receptor-modelling techniques; these sources of particulate matter were biomass combustion, motor vehicles, secondary sulphate, marine aerosol and soil. The primary source of peak winter $PM_{2.5}$ in Hastings was the biomass combustion source, which was attributed to the use of solid fuel fires for home heating and contributed 80% of the total $PM_{2.5}$ mass during peak concentrations (>15 μg m^{-3}). Contributions to peak PM_{10} concentrations reflected the influence of $PM_{2.5}$ combustion sources, along with a greater influence of coarse-particle sea salt and crustal matter. The biomass-combustion source was found to be contaminated with arsenic and lead due to the use of copper chrome arsenate (CCA)-treated timber and old painted timber, respectively, as fuel.

Key results from the study are:

1. $PM_{2.5}$ concentrations were highest during winter and the primary driver of peak PM_{10} concentrations over the same time period; this was indicative of the sources contributing to particulate-matter concentrations at Hastings.
2. Five distinct source types were extracted from the data. These were: biomass combustion, motor vehicles, secondary sulphate, marine aerosol (sea salt) and soil (crustal matter) and is a similar result to previous studies. Figures ES.1 and ES.2 present the relative source contributions to $PM_{2.5}$ and PM_{10}, respectively.
3. Biomass combustion was the primary source of fine particulate matter in Hastings, contributing to 69% of $PM_{2.5}$ over the monitoring period, and most of this occurred during winter. The contribution from this source on peak pollution days was found to be typically 80% of $PM_{2.5}$ concentrations.
4. As the PM_{10} size fraction contains $PM_{2.5}$, biomass combustion was also the dominant contributor to PM_{10} during winter but, at other times of the year for both size fractions, crustal matter (soil), secondary sulphate and natural marine aerosol were the primary sources.

It was found that contributions from motor vehicles and crustal-matter sources increased (approximately 0.5 μg m^{-3}) in the aftermath of the flooding and silt from Cyclone Gabrielle, and this was likely due to increases in road dust from the passage of motor vehicles on local roads and wind-blown crustal matter at higher wind speeds (>10 m/s). However, the increase in crustal-matter contributions was offset by a significant decrease in marine-aerosol and secondary-sulphate contributions (approximately 4 μg m^{-3}) over the same time period. Contributions from biomass-combustion sources were relatively similar across the three winters (2022, 2023 and 2024).

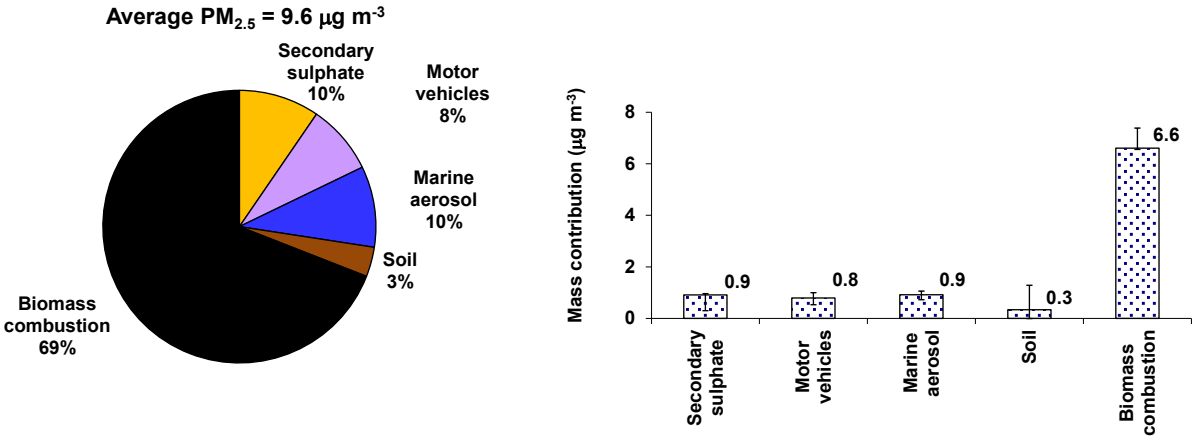

Figure ES.1 Average source contributions to $PM_{2.5}$ at Hastings over the monitoring period (May 2023 to August 2024).

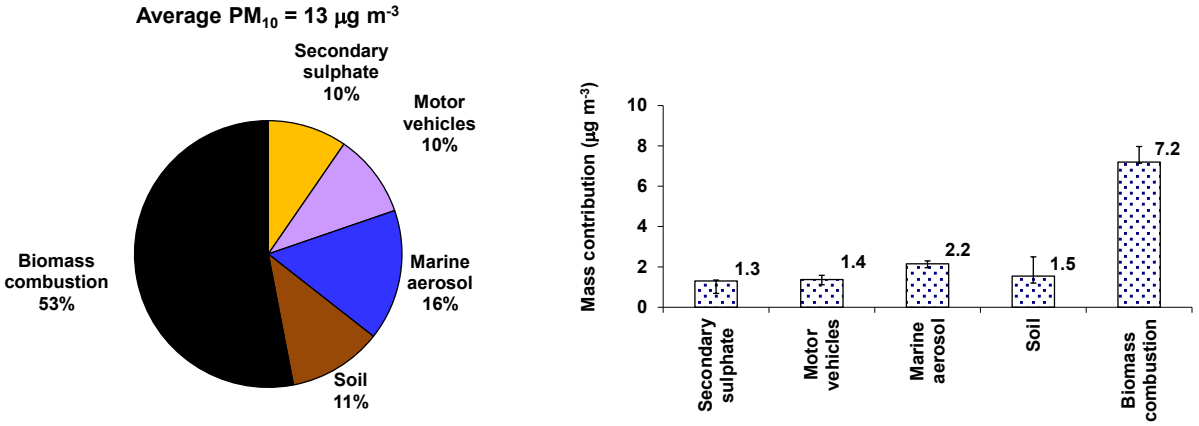

Figure ES.2 Average source contributions to PM_{10} at Hastings over the monitoring period (May 2023 to August 2024).

While the results from the monitoring indicate that crustal-matter 'dust' events resulting in high airborne particulate-matter concentrations (i.e. close to the $PM_{2.5}$ World Health Organization Guideline or the PM_{10} National Environmental Standard) were not captured at the monitoring site in the wake of the Cyclone Gabrielle aftermath, localised dust nuisance may have occurred elsewhere in the airshed, particularly around activities that involved soil disturbance. Soil particles, being relatively large and heavy, are likely to settle out of the atmosphere rapidly downwind of a re-suspension source unless there are significant wind speeds at the same time to carry finer particles further afield.

1.0 INTRODUCTION

This report presents the results of a compositional analysis and receptor-modelling study of airborne particle samples collected during 2023 and 2024 at an ambient air-quality monitoring site in Hastings, Hawke's Bay. The study was initiated to assess the impact that the aftermath of Cyclone Gabrielle had on the Hastings airshed, particularly due to the large amounts of silt deposited by the associated flooding. The potential for clean-up activities and wind action to result in high airborne-dust concentrations was of interest to Hawke's Bay Regional Council as part of its ambient air-quality monitoring programme and the requirement to manage air quality in the region.

The work also follows on from a sampling, compositional analysis and receptor-modelling study of $PM_{2.5}$ and PM_{10} that ran from April 2022 until April 2023 (Davy and Trompetter 2023) and provides the opportunity to compare source contributions at the monitoring site before and after the impact of Cyclone Gabrielle.

Sampling and sample analysis for the current work was funded by the Cyclone Gabrielle Response Fund administered by NIWA (National Institute of Water & Atmospheric Research), while the data analysis and reporting was funded through an Envirolink grant (Hawke's Bay Regional Council advice number HBRC202401).

1.1 Requirement to Manage Airborne-Particle Pollution

In 2004, in response to growing evidence of significant health effects associated with airborne-particle pollution, the New Zealand Government introduced a National Environmental Standard (NES) of 50 $\mu g/m^3$ (24-hour average) for particles less than 10 μm in aerodynamic cross-section (denoted as 'PM_{10}'). The NES places the onus on regional councils to monitor PM_{10} and publicly report whether the air quality in their region exceeds the standard, with a provision for no more than one exceedance annually and a requirement for offsets by industry in PM_{10}-polluted airsheds replacing the restriction on industrial consents (Ministry for the Environment 2011). Air pollution episodes that are outside regulatory authorities' ability to control may be considered 'exceptional events' by application for exemption (e.g. dust storms, volcanic eruptions).

In areas where the PM_{10} standard is exceeded, information on the sources contributing to those air-pollution episodes is required to:

- identify 'exceptional events' outside of regulatory authority control;
- effectively manage air quality; and
- formulate appropriate mitigation strategies, where necessary.

In addition to the PM_{10} NES, the Ministry for the Environment issued ambient air-quality guidelines (AAQGs) for air pollutants in 2002 that included a (monitoring) guideline value of 25 $\mu g\ m^{-3}$ for $PM_{2.5}$ (24-hour average). More recently, the World Health Organization (WHO) has confirmed a $PM_{2.5}$ AAQG value of 15 $\mu g\ m^{-3}$ (24-hour average) based on the relationship between 24-hour and annual particulate-matter levels (WHO 2021). The WHO annual average guideline for $PM_{2.5}$ is 5 $\mu g\ m^{-3}$. These are the lowest levels at which total, cardiopulmonary and lung cancer mortality have been shown to increase (at the 95% confidence intervals) in response to exposure to $PM_{2.5}$. WHO recommends the use of $PM_{2.5}$ guidelines over PM_{10}, as epidemiological studies have shown that most of the adverse health effects associated with PM_{10} are due to $PM_{2.5}$. A recent analysis of the impact of air pollution on human health in New Zealand found that residential wood burning dominated the health effects associated with $PM_{2.5}$ pollution (Kuschel et al. 2022).

1.1.1 Identifying Sources of Airborne-Particle Pollution Analysis

Measuring the mass concentration of air particulate matter provides little information on the identity of the contributing sources. Airborne particles are composed of many elements and compounds from many different sources. Receptor modelling provides a means to determine the relative mass contribution of sources that impact significantly on the total mass of air particulate matter collected at a monitoring site. Elemental concentrations in particulate-matter filter samples were determined using accelerator-based Ion Beam Analysis (IBA) techniques at the New Zealand Ion Beam Analysis Facility in Gracefield, Lower Hutt. Black carbon concentrations were determined using light-reflectance techniques.

IBA is a mature analytical technique that provides a non-destructive determination of multi-elemental concentrations present in a sample. Using elemental concentrations with appropriate statistical techniques and purpose-designed mathematical models, the sources contributing to each ambient sample can be estimated. Appendix 1 provides a description of the IBA analytical process and receptor-modelling techniques.

1.1.2 Scope of this Study

This report describes sampling, results and outcomes according to the following objectives:

- Identify the sources contributing to air-pollution episodes.
- Identify the sources responsible for the emission of toxic contaminants.
- Estimate the contribution of soil, sea salt and other natural particulate-matter sources to ambient concentrations.
- Estimate the contribution of secondary particulate-matter sources to ambient concentrations.
- Distinguish between the contribution of home-heating and motor-vehicle emission sources.
- Determine the variation of source contributions by season.
- Intercompare the results for the $PM_{2.5}$ and PM_{10} samples.
- Assess the effects on air quality from the impact of Cyclone Gabrielle.

2.0 METHODOLOGY

2.1 Location of the Hastings Particulate-Matter Monitoring Site

Particulate matter ($PM_{2.5}$ and $PM_{10–2.5}$) sampling was undertaken by Hawke's Bay Regional Council from May 2023 until August 2024 at its air-quality monitoring station on the grounds of St Johns College, Hastings (latitude -39.6390, longitude 176.8588). The site is located in the middle of a residential area, as shown in Figure 2.1.

The authors have been provided with information about the monitoring site and informed of the typical activities in the surrounding areas that may contribute to particulate-matter concentrations. These details informed the conceptual receptor model described in Section 2.5.

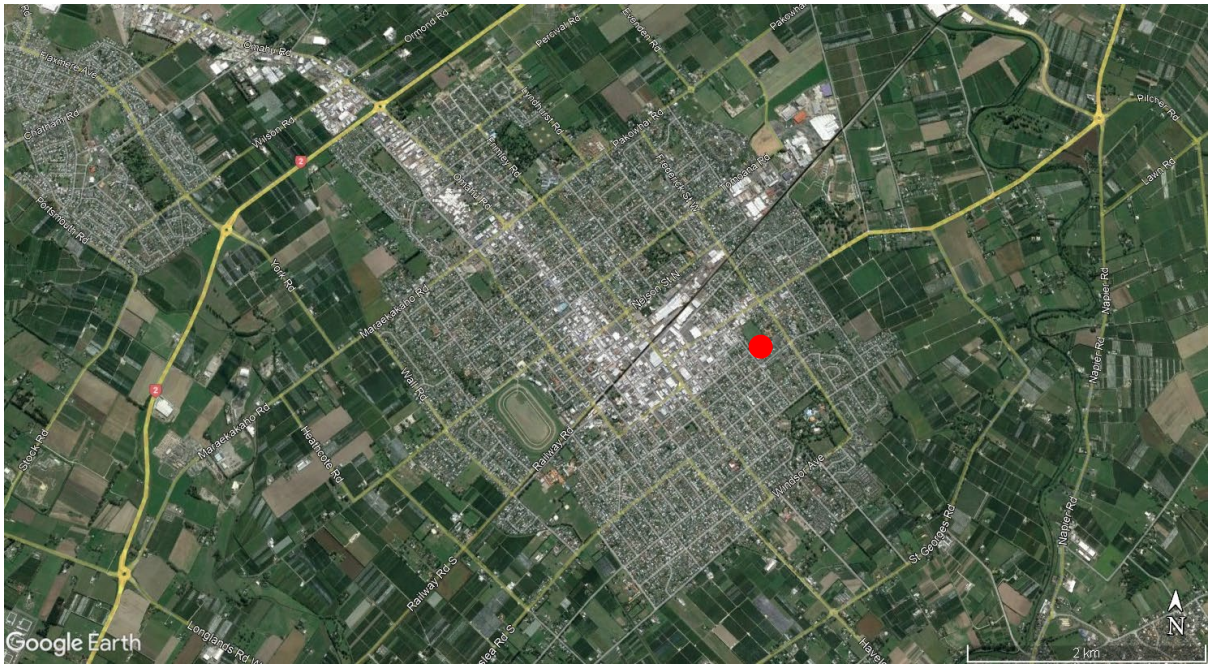

Figure 2.1 Location of Hastings monitoring site (●). (Image source: Google Earth 2023).

The area immediately around the site is flat and predominately residential, with local urban road traffic. Hastings town centre and commercial area lies to the west and northwest of the site. Further residential suburbs lie to the north and south. The coast (Hawke Bay) is approximately 10 km directly east. Land use surrounding the Hastings urban area is predominantly agricultural.

2.2 Description of Particulate-Matter Sampling at Hastings

Particulate-matter samples (12-hour time-integrated sampling period) for analysis were collected onto Streaker filter wheels at the Hastings air-quality monitoring site using a Streaker sampler (PIXE International Inc. Tallahassee, USA). A total of 836 $PM_{2.5}$ and $PM_{10–2.5}$ samples were collected on a 12-hourly (18:00–06:00 and 06:00–18:00) continuous sampling regime over the monitoring period. All particulate-matter sampling and systems maintenance at the air-quality monitoring site was carried out by Hawke's Bay Regional Council, and, as such, it maintains all records of equipment, flow rates and sampling methodologies used for its continuous particulate-matter sampling at the site.

2.3 Receptor-Modelling Process

The multivariate analysis of air particulate-matter sample composition (also known as receptor modelling) provides groupings (or factors) of elements that vary together over time. This technique effectively provides a chemical 'fingerprint' for each source that contributes to airborne particulate matter collected at the site and the mass of each element (as well as the particulate-matter mass) attributed to that source. In this study, the primary source contributors were determined using results from the Positive Matrix Factorisation (PMF) analysis of the particulate-matter elemental composition.

A critical point for understanding the receptor-modelling process is that the PMF model can produce any number of solutions, all of which may be mathematically correct (Paatero et al. 2002). The 'best' solution (e.g. number of factors, etc.) is generally determined by the practitioner after considering the model diagnostics and a review of the available factor profiles and contributions (to check physical interpretability). Most commonly used receptor models are based on conservation of mass from the point of emission to the point of sampling and measurement (Hopke 1999). Their mathematical formulations express ambient chemical concentrations as the sum of products of species abundances in source emissions and source contributions. In other words, the chemical profile measured at a monitoring station is resolved mathematically to be the sum of a number of different factors or sources. As with most modelling approaches, receptor models based on the conservation of mass are simplifications of reality and have the following general assumptions:

1. Compositions of source emissions are constant over the period of ambient and source sampling.
2. Chemical species do not react with each other (i.e. they add linearly).
3. All sources with a potential for contributing to the receptor have been identified and had their emissions characterised.
4. The number of sources or source categories is less than or equal to the number of species measured.
5. The source profiles are linearly independent of each other.
6. Measurement uncertainties are random, uncorrelated and normally distributed.

The effects of deviations from these assumptions are testable and can therefore allow the accuracy of source quantification to be evaluated. Uncertainties in input data can also be propagated to evaluate the uncertainty of source contribution estimates. There are a number of natural physical restraints that must be considered when developing a model for identifying and apportioning sources of airborne particles; these are (Hopke 2003):

- The model must explain the observations.
- The predicted source compositions must be non-negative.
- The predicted source contributions must be non-negative.
- The sum of predicted elemental mass contributions from each source must be less than or equal to measured mass for each element.

These constraints need to be kept in mind when conducting and interpreting any receptor modelling approach, particularly as a receptor model is still an approximation of the real-world system. Several factors also affect the nature of a source's particle composition and its contributions to ambient loadings (Brimblecombe 1986; Hopke 1999; Seinfeld and Pandis 2006):

1. The composition of particles emitted from a source may vary over time.
2. The composition of particles is modified in the atmosphere through a multitude of processes and interactions, for example:
   - Adsorption of other species onto particle surfaces.
   - Gas-to-particle conversions forming secondary particulate matter, for example, the conversion of SO_2 gas to SO_4^{2-}.
   - Volatilisation of particle components, such as organic compounds, or volatilisation of chlorine through reaction with acidic species.
   - Interaction with, and transformation by, solar radiation and free radicals in the atmosphere, such as the OH and NO_3 species.

The analytical processes used in this study did not analyse for nitrate (elemental hydrogen, carbon, oxygen and nitrogen are not detectable by the IBA techniques used), so the missing mass that the analysis is not explaining is likely a combination of nitrate and other unmeasured species, such as hydrocarbons and bound water. Measurement of the ionic components in PM_{10} at other New Zealand sites indicates that aerosol nitrate species (primarily as $PM_{2.5}$) contribute approximately 0.25 μg m^{-3} in Auckland (Ancelet and Davy 2015) and 0.75 μg m^{-3} in Timaru (Scott 2014) to total particulate-matter mass during winter and somewhat less during other seasons due to atmospheric processing and thermodynamic equilibria (Seinfeld and Pandis 2006).

Analytical noise is also introduced during the species-measurement process, such as analyte interferences and limits of detection for species of interest. These are at least in the order of 5% for species well above their respective detection limits and 20% or more for those species near the analytical method detection limit (Hopke 1999). Further details on data analysis and dataset preparation are provided in Appendix 1.

2.4 Data Analysis and Reporting

The receptor-modelling results within this report have been produced in a manner that provides as much information as possible on the relative contributions of sources to particulate-matter concentrations so that this may be used for monitoring strategies, air-quality management and policy development. The data have been analysed to provide the following outputs:

1. Masses of elemental species apportioned to each source.
2. Source chemical profiles.
3. Average particulate-matter mass apportioned to each source.
4. Temporal variations in source mass contributions (time-series plots).
5. Seasonal variations in source mass contributions. For the purposes of this study, summer has been defined as December–February, autumn as March–May, winter as June–August and spring as September–November.
6. Analysis of source contributions on peak particulate-matter days.
7. Identification of sources of any particulate matter that may be related to the aftermath of Cyclone Gabrielle.

Table 2.1 presents the relevant standards, guidelines and targets for particulate matter concentrations.

Table 2.1 Standards, guidelines and targets for particulate-matter concentrations.

Particle Size	Averaging Time	Ambient Air Quality Guidelines [1] (µg m^{-3})	'Acceptable' Air Quality Category [2] (µg m^{-3})	'Alert' Air Quality Category [2] (µg m^{-3})	National Environmental Standard (µg m^{-3})
PM_{10}	24 hours	50	<33	>33 <50	50
	Annual	20	<13	>13 <20	-
$PM_{2.5}$	24 hours	25	<17	>17 <25	-

[1] Ministry for the Environment (2002).

[2] Air-quality categories taken from Ministry for the Environment (1997).

2.4.1 Conditional Probability Function Analysis

A useful data-analysis method is to investigate the relationship between the source contributions and wind direction. Bivariate polar plots using the source contributions to particulate matter were produced using R statistical software and the *openair* package (Carslaw 2012; Carslaw and Ropkins 2012; R Core Team 2015). Using bivariate polar plots, source contributions can be shown as a function of both wind speed and direction, providing invaluable information about potential source regions and how pollution from a specific source builds up. To produce the polar plots, wind speeds and directions were vector-averaged using functions available in *openair*. A full description of the vector-averaging process can be found in Carslaw (2012).

Conditional Probability Function (CPF) analysis provides a method to find the directions for which high values of source contributions are likely to be related (Ashbaugh et al. 1985). The probability that a source contribution originates from a given wind direction is estimated by comparing the wind direction distribution for the upper 25% of source contributions relative to the total wind-direction distribution.

$$CPF_{\Delta\theta} = \frac{m_{\Delta\theta}}{n_{\Delta\theta}}$$

where:

- $m_{\Delta\theta}$: number of occurrences from wind sector $\Delta\theta$ for the upper 25% of source contributions.
- $n_{\Delta\theta}$: total number of occurrences from the same wind sector.

Sources are likely to be located in the directions that have high CPF values. Because of the smoothing involved, the colour scale is only to provide an indication of overall pattern and should not be interpreted in concentration units.

2.5 Conceptual Receptor Model for Particulate Matter at Hastings

An important part of the receptor-modelling process is to formulate a conceptual model of the receptor site. This means understanding and identifying the major sources that may influence ambient particulate-matter concentrations at the site. For the Hastings site, the initial conceptual model includes local emission sources:

- Domestic activities – likely to be dominated by biomass-combustion activities such as emissions from solid-fuel fires used for domestic heating during the winter.
- Motor vehicles – all roads in the area act as line sources, and roads with higher traffic densities will dominate emissions.
- Industrial emissions from combustion processes (boilers) and dust-generating activities such as excavation, construction and bulk-storage handling.
- Local wind-blown soil or road dust sources may also contribute. Specifically for the Hawke's Bay region, the flooding and devastation wrought by Cyclone Gabrielle during mid-February 2023 left large areas of the surrounding countryside, including roads, covered in layers of silt.

Sources that originate further from the monitoring site would also be expected to contribute to ambient particle loadings. These include:

- Marine aerosol (sea salt) generated in the oceanic regions around New Zealand.
- Secondary particulate matter resulting from atmospheric gas-to-particle conversion processes – this includes sulphates, nitrates and organic species.

Another category of emission sources that may contribute are those considered to be 'one-off' emission sources:

- Fireworks displays and other special events (e.g. Guy Fawkes Day).
- Short-term road works and demolition/construction activities.

The variety of sources described above can be recognised and accounted for using appropriate data-analysis methods, such as the application of geochemical principles, the examination of seasonal differences and temporal variations and the receptor modelling itself.

2.6 Local Meteorology at Hastings

A meteorological station owned and operated by Hawke's Bay Regional Council was located at the air-quality monitoring site. As shown in Figure 2.2, the predominant wind directions were from the southerly quadrant for the monitoring period (May 2023 – August 2024). Seasonal differences in wind speed and direction were evident as presented in Figure 2.3. Winds were stronger and predominantly from the south during autumn and winter, with a greater percentage of north to northeasterly winds during spring and summer.

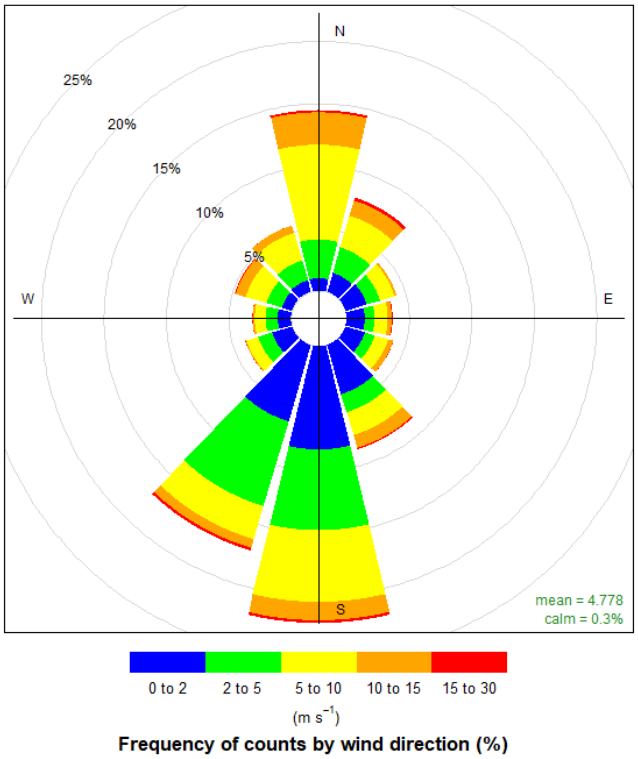

Figure 2.2 Wind rose for the monitoring period at Hastings (May 2023 – August 2024).

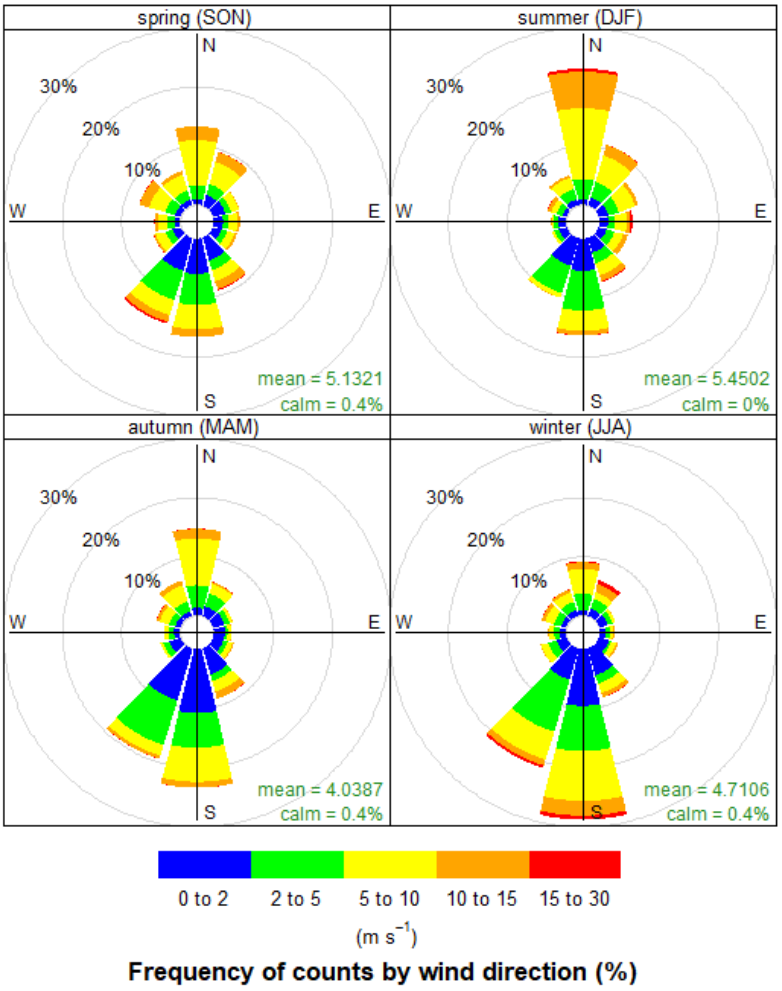

Figure 2.3 Seasonal wind roses for the monitoring period at Hastings (May 2023 – August 2024).

2.7 $PM_{2.5}$ and PM_{10} Concentrations at Hastings

Due to the type of filters used by the Streaker sampler, gravimetric mass concentrations for $PM_{2.5}$ and PM_{10} were not determined – instead, the Hastings $PM_{2.5}$ and PM_{10} concentrations from continuous monitoring instruments (Fidas light-scattering aerosol spectrometer, Palas GmbH, Germany) were used as the particle-matter mass concentration variable in the receptor modelling. Figures 2.4 and 2.5 present the $PM_{2.5}$ and PM_{10} monitoring results (24-hour averages, midnight-to-midnight sampling regime) over the monitoring period (May 2023 – August 2024). Gaps present in Figures 2.4 and 2.5 are from sampler outages and/or maintenance. The WHO AAQG concentration (15 µg m^{-3} as a 24-hour average) for $PM_{2.5}$ was exceeded on 92 occasions during the monitoring period, all of these during winter months. The National Environment Standard Air Quality standard (NESAQ) for PM_{10} was exceeded three times during the filter sampling campaign (note that more exceedances for both $PM_{2.5}$ and PM_{10} may have been captured by the continuous monitoring instruments).

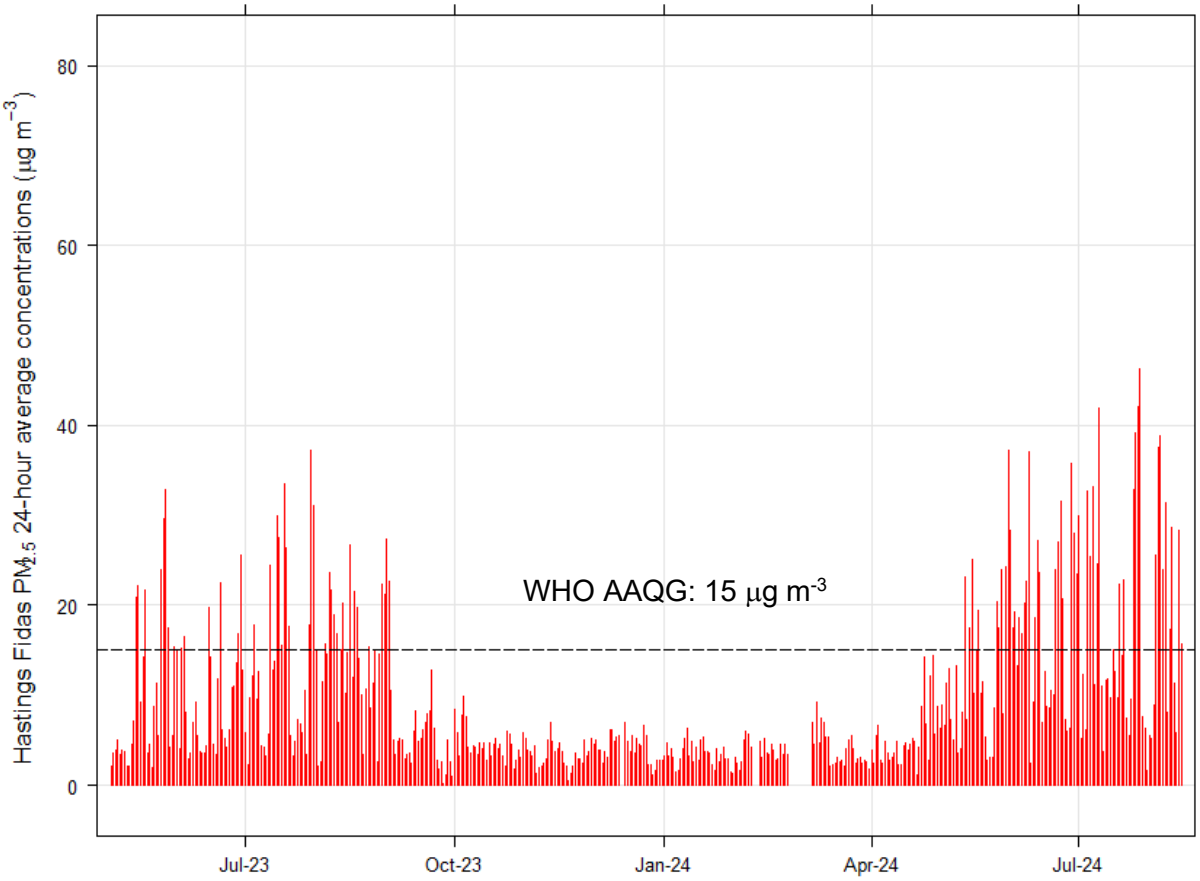

Figure 2.4 Fidas (nephelometer) continuous monitoring $PM_{2.5}$ (24-hour average) concentrations at Hastings. Note that the gaps in the graph are due to missing samples. The dashed line indicates the WHO AAQG concentration (15 µg m^{-3} as a 24-hour average) for $PM_{2.5}$.

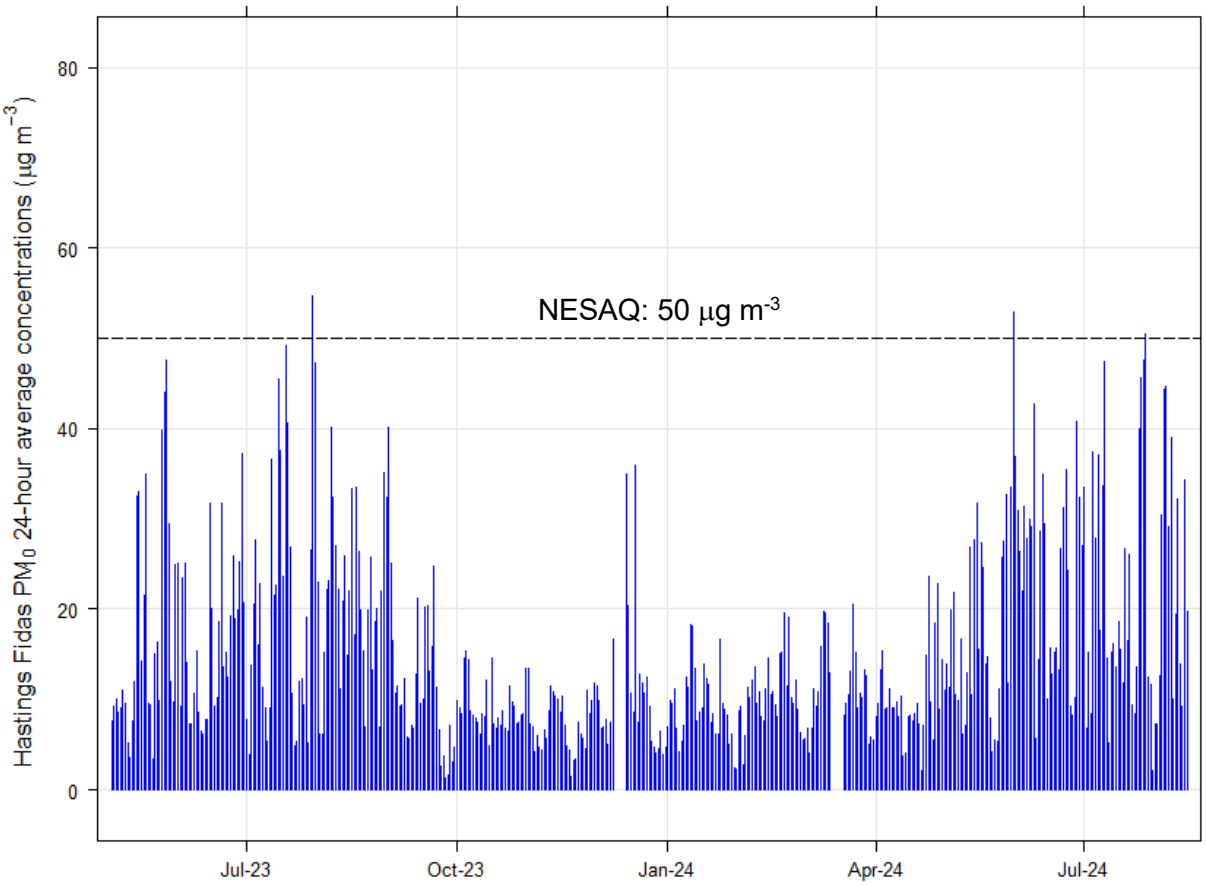

Figure 2.5 Fidas (nephelometer) continuous monitoring PM_{10} (24-hour average) concentrations at Hastings. Note that the gaps in the graph are due to missing samples. The dashed line indicates the NESAQ standard for PM_{10}.

Figures 2.4 and 2.5 show that $PM_{2.5}$ and PM_{10} concentrations at Hastings have a seasonal pattern, with peak concentrations during winter. This pattern is likely to be explained by the types of sources contributing to particulate-matter concentrations at the site.

3.0 RECEPTOR-MODELLING ANALYSIS OF HASTINGS PARTICULATE-MATTER SOURCES

3.1 Analysis of Particulate-Matter Samples Collected at Hastings

$PM_{2.5}$ and $PM_{10–2.5}$ samples at Hastings were collected by Hawke's Bay Regional Council using a Streaker sampler system on a 12-hour sampling regime over the monitoring period. Overall, a total of 836 $PM_{2.5}$ and 836 $PM_{10–2.5}$ samples were collected from May 2023 to August 2024. Elemental and black carbon concentrations in the particulate-matter samples were determined using IBA and light reflection, respectively, as described in Appendix 1.

3.1.1 Composition of $PM_{2.5}$ at Hastings

Elemental concentrations in the $PM_{2.5}$ samples collected at the Hastings monitoring site are presented in Table 3.1. The data show that $PM_{2.5}$ concentrations are dominated by black carbon, with peak concentrations during the winter months. Other important elemental constituents included K, Na, Cl, Si, Al, S and Fe, indicating that combustion sources, marine aerosol, crustal matter and secondary-sulphate particles were likely to be important contributors to $PM_{2.5}$ concentrations at the monitoring site. Some measured species were close to or below their respective limit of detection (LOD) in each of the samples. Appendix 1 provides a description of data treatment and detection limits. Elemental correlation plots are provided in Figure A2.2.

Table 3.1 Elemental concentrations in $PM_{2.5}$ samples from Hastings (836 samples).

	Unit	Average	Maximum	Minimum	Median	Std. Dev.	Average LOD	% > LOD
$PM_{2.5}$	µg m^{-3}	10	98	0	5	15	-	-
Black Carbon	ng m^{-3}	936	6840	14	518	1154	91	96
Na	ng m^{-3}	88	802	0	74	74	152	16
Mg	ng m^{-3}	16	104	0	14	11	5	92
Al	ng m^{-3}	15	228	0	8	21	3	91
Si	ng m^{-3}	41	676	0	19	61	2	95
P	ng m^{-3}	4	21	0	4	3	2	95
S	ng m^{-3}	59	417	0	47	54	1	95
Cl	ng m^{-3}	111	1848	0	39	173	1	91
K	ng m^{-3}	88	1176	0	34	145	1	99
Ca	ng m^{-3}	21	218	2	16	17	1	100
Sc	ng m^{-3}	1	7	0	0	1	1	18
Ti	ng m^{-3}	1	14	0	1	2	1	39
V	ng m^{-3}	0	5	0	0	0	1	6
Cr	ng m^{-3}	1	9	0	1	1	1	79
Mn	ng m^{-3}	1	41	0	0	2	1	36
Fe	ng m^{-3}	15	264	1	8	20	0	100
Co	ng m^{-3}	0	3	0	0	0	1	14
Ni	ng m^{-3}	0	3	0	0	0	1	24

	Unit	Average	Maximum	Minimum	Median	Std. Dev.	Average LOD	% > LOD
Cu	ng m^{-3}	1	101	0	1	6	1	50
Zn	ng m^{-3}	6	87	0	3	9	1	85
Ga	ng m^{-3}	0	5	0	0	0	1	3
Ge	ng m^{-3}	0	5	0	0	1	2	4
As	ng m^{-3}	5	84	0	1	9	3	44
Se	ng m^{-3}	0	11	0	0	1	3	4
Br	ng m^{-3}	3	274	0	1	12	4	23
Rb	ng m^{-3}	1	35	0	0	3	8	3
Sr	ng m^{-3}	1	36	0	0	3	10	2
Mo	ng m^{-3}	4	105	0	0	11	36	3
I	ng m^{-3}	2	24	0	1	3	6	20
Ba	ng m^{-3}	2	97	0	1	5	4	11
Hg	ng m^{-3}	1	17	0	0	2	4	3
Pb	ng m^{-3}	2	57	0	0	6	8	6

3.1.2 Composition of $PM_{10–2.5}$ at Hastings

Elemental concentrations in the $PM_{10–2.5}$ samples collected at the Hastings monitoring site are presented in Table 3.2. Elemental constituents such as, Na, Cl, Si, Al, S and Fe were significantly higher in $PM_{10–2.5}$, indicating that coarse particle ($PM_{10–2.5}$ fraction) sources, such as marine aerosol and crustal matter, were likely to be important contributors to $PM_{10–2.5}$ concentrations at the monitoring site, in addition to the $PM_{2.5}$ sources described in Section 3.1.1.

Table 3.2 Elemental concentrations in $PM_{10–2.5}$ samples from Hastings (836 samples).

	Unit	Average	Maximum	Minimum	Median	Std. Dev.	Average LOD	% > LOD
$PM_{10–2.5}^{*}$	µg m^{-3}	4.7	28	0.0	4.2	3.4	-	-
Na	ng m^{-3}	467	2532	0	331	438	152	77
Mg	ng m^{-3}	76	401	0	62	57	5	99
Al	ng m^{-3}	72	499	0	51	69	2	100
Si	ng m^{-3}	244	1935	0	176	240	2	100
P	ng m^{-3}	7	102	0	6	6	2	97
S	ng m^{-3}	77	877	0	63	60	2	100
Cl	ng m^{-3}	878	4798	0	676	744	1	100
K	ng m^{-3}	61	301	0	52	40	1	100
Ca	ng m^{-3}	98	778	0	81	75	1	100
Sc	ng m^{-3}	1	10	0	1	1	1	35
Ti	ng m^{-3}	6	40	0	5	6	1	98
V	ng m^{-3}	0	4	0	0	0	1	11
Cr	ng m^{-3}	1	28	0	0	1	0	58

	Unit	Average	Maximum	Minimum	Median	Std. Dev.	Average LOD	% > LOD
Mn	ng m^{-3}	1	8	0	1	1	0	81
Fe	ng m^{-3}	67	420	0	46	54	1	100
Co	ng m^{-3}	1	7	0	0	1	1	16
Ni	ng m^{-3}	0	9	0	0	1	0	10
Cu	ng m^{-3}	2	25	0	1	2	1	75
Zn	ng m^{-3}	3	26	0	2	3	1	90
Ga	ng m^{-3}	0	4	0	0	0	1	2
Ge	ng m^{-3}	0	3	0	0	0	1	1
As	ng m^{-3}	0	6	0	0	1	2	4
Se	ng m^{-3}	0	6	0	0	1	2	1
Br	ng m^{-3}	2	50	0	1	4	3	31
Rb	ng m^{-3}	0	12	0	0	1	5	1
Sr	ng m^{-3}	1	25	0	0	2	6	2
Mo	ng m^{-3}	1	54	0	0	4	19	0
I	ng m^{-3}	2	25	0	1	3	9	5
Ba	ng m^{-3}	2	24	0	2	3	4	18
Hg	ng m^{-3}	1	19	0	0	2	3	8
Pb	ng m^{-3}	0	33	0	0	2	4	1

* Note that the $PM_{10–2.5}$ mass concentration data has been generated by subtracting the $PM_{2.5}$ concentrations from PM_{10}.

3.2 Source Contributions to Particulate Matter at Hastings

The $PM_{2.5}$ and $PM_{10–2.5}$ compositional data were analysed to provide information on contributing sources using PMF with multiple re-iterations to achieve robust solutions and source attributions. Sources of particulate-matter emissions or generation include particles across the size-range spectrum and therefore contribute to both fine- and coarse-size fractions, although some source types will contribute more to one size fraction than the other. For example, combustion sources, such as domestic solid-fuel fires or motor-vehicle tail-pipe emissions, produce particles in the sub-micron size range and are therefore largely confined to the $PM_{2.5}$ fraction. Windblown dust; road dust generated by the turbulent passage of motor vehicles over local roads; sea salt; or industrial processes that involve mechanical grinding, sorting, storage and transport of bulk materials, predominantly produce particles in the larger size ranges (>$PM_{2.5}$) although some 'tail' of particle sizes does extend down into the $PM_{2.5}$ size fraction.

3.2.1 Sources of $PM_{2.5}$ at Hastings

Five source types were identified from PMF receptor-modelling analysis of the Hastings $PM_{2.5}$ elemental data. Table 3.3 and Figure 3.1 present the source elemental profiles and $PM_{2.5}$ contributions extracted from the PMF analysis. The source contributors identified were found to explain 91% of the $PM_{2.5}$ mass on average.

The sources identified were:

- **Biomass combustion:** The first factor was identified as biomass combustion based on the dominance of black carbon and K in the profile (Fine et al. 2001; Khalil and Rasmussen 2003). Trace amounts of As and Pb were also strongly associated with the biomass-combustion profile. The presence of these heavy metals associated with the biomass-combustion source is consistent with previous monitoring results at Hastings (Wilton et al. 2007; Davy and Trompetter 2023) and throughout New Zealand (Davy et al. 2014), indicating co-combustion of copper chrome arsenate (CCA)-treated timber and old painted timber, respectively, as fuels.
- **Motor vehicles:** The second factor was identified as motor vehicles because of the presence of black carbon, Fe, Cu and Zn as significant elemental components. This profile is likely a combination of tail-pipe (black carbon and Zn from fuel combustion) and re-entrained road-dust emissions (Al, Si, Ca, Ti and Fe crustal-matter components, Cu from brake dust).
- **Secondary sulphate:** The third factor was identified as a secondary-sulphate source because of the dominance of sulphur in the profile. This source contribution was likely to be from secondary-sulphate aerosol produced in the atmosphere from gaseous precursors.
- **Marine aerosol:** The fourth factor was identified as a marine aerosol source because of the predominance of Na and Cl, along with Mg, S, K and Ca in similar ratios to sea water.
- **Soil:** A fifth source was identified for $PM_{2.5}$ as originating from activities that generate crustal matter. Crustal matter is primarily composed of aluminosilicate minerals, and the source profiles extracted from receptor modelling reflect this, with Al and Si being the primary constituents and Mg, K, Ca, Ti and Fe also present.

Further analysis of the $PM_{2.5}$ source contributors is provided in the following sections.

Table 3.3 Average source elemental concentration profiles for $PM_{2.5}$ samples from Hastings (based on 836 samples). All units are in ng m^{-3}.

	Biomass Combustion	Motor Vehicles	Secondary Sulphate	Marine Aerosol	Soil
$PM_{2.5}$	6600	790	910	920	340
BC	1439	380	0.0	65	25.0
Na	18.7	31.1	44.3	393.5	9.6
Mg	4.4	1.7	0.6	29.3	2.3
Al	3.2	3.5	4.2	10.9	11.4
Si	4.0	11.1	10.3	4.8	35.3
S	15.2	0.0	75.4	34.1	4.6
Cl	40.3	0.0	0.0	481.2	1.6
K	68.1	1.4	10.3	10.3	5.8
Ca	0.0	1.1	0.7	7.1	8.4
Ti	0.0	1.2	0.0	0.1	0.8
Fe	1.8	6.0	1.8	0.0	8.4
Cu	0.4	0.5	0.2	0.1	0.1
Zn	4.1	1.2	0.9	0.0	0.4
As	3.9	0.1	0.0	0.1	0.2
Pb	3.2	0.5	0.7	0.1	0.0

Table 3.3 shows that biomass combustion continues to be the dominant contributing source to average $PM_{2.5}$ concentrations at Hastings, primarily during winter. Note that the summation of elemental components does not equal particulate-matter mass, as this analysis was not for compounds (which includes oxides and other unmeasured species, as described in Section 2.1) but for proportional elemental co-variance and the proportion of particulate-matter mass that is also co-variant with those elemental species.

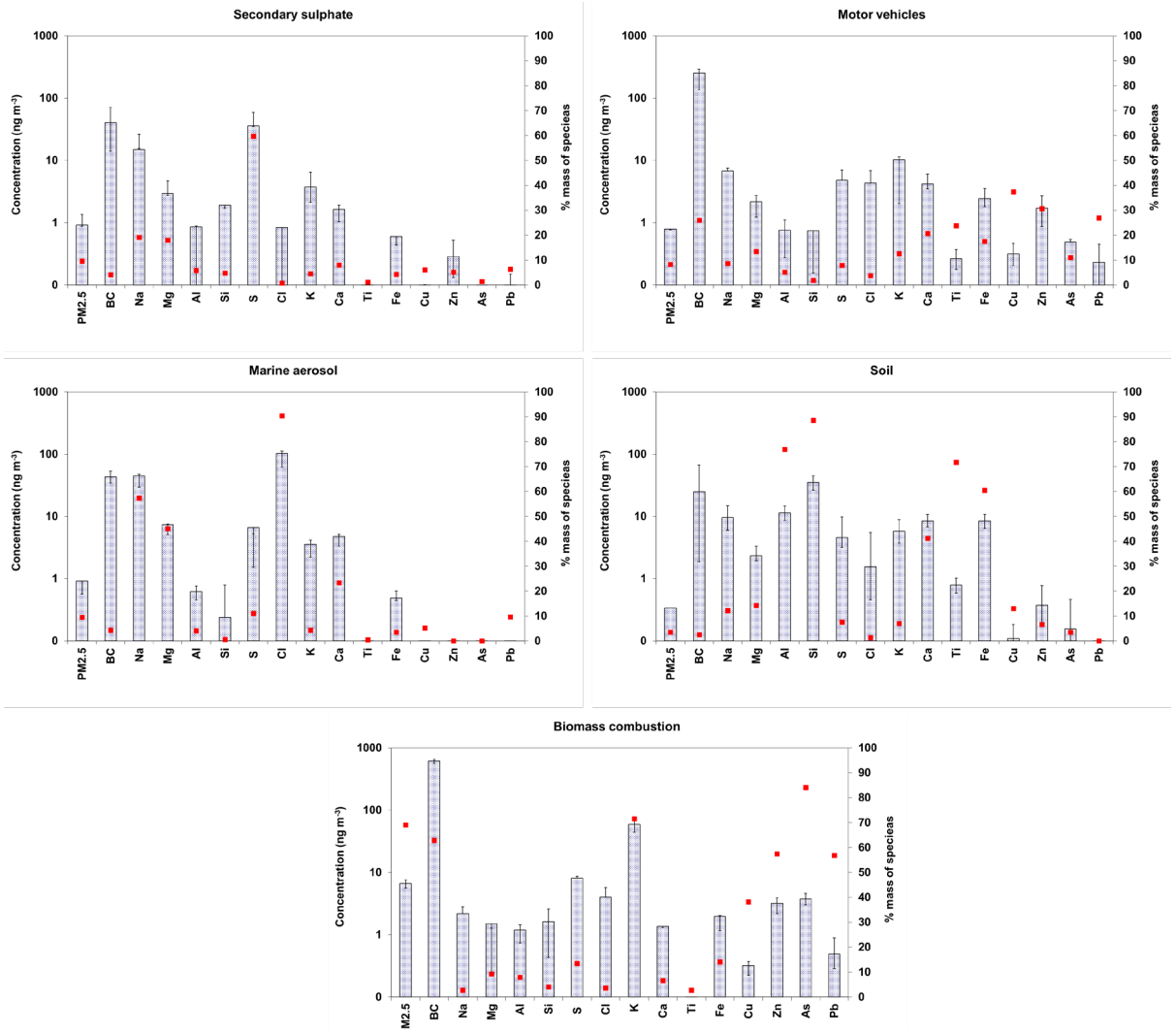

Figure 3.1 Source elemental concentration profiles for $PM_{2.5}$ samples from Hastings. The red dots represent the percentage of each chemical species attributed to each source.

Figure 3.2 presents the relative source contributions to $PM_{2.5}$ in Hastings. Also included are the 5th and 95th percentile confidence limits (bottom and top of error bar, respectively) in average mass contributions attributed to each of the sources, indicating the variability in average mass contributions over the monitoring period. Note that $PM_{2.5}$ refers to the measured gravimetric mass on the filter samples, while 'BAM $PM_{2.5}$' refers to the beta-attenuation monitor measurement of $PM_{2.5}$ for the same sampling period.

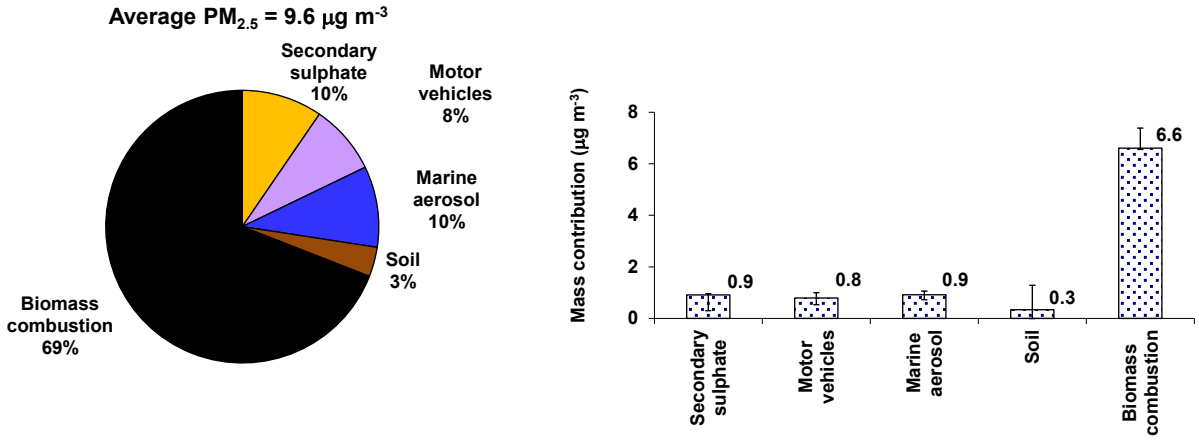

Figure 3.2 Average source mass contributions to $PM_{2.5}$ at Hastings over the monitoring period May 2023 to August 2024.

The average $PM_{2.5}$ source contributions over the entire monitoring period (note that the sampling included two winters) estimated from the PMF analysis showed that biomass combustion (69%) was the most significant contributor to $PM_{2.5}$ mass, with marine aerosol (10%) and secondary sulphate (10%) the next highest, while motor vehicles (8%) and crustal matter (3%) had the lowest contributions to $PM_{2.5}$ mass.

3.2.2 Sources of $PM_{10–2.5}$ at Hastings

Two source types were identified from PMF receptor-modelling analysis of the Hastings $PM_{10–2.5}$ elemental data. Table 3.4 and Figure 3.3 present the source elemental profiles and $PM_{10–2.5}$ contributions extracted from the PMF analysis. The source contributors identified were found to explain 97% of the $PM_{10–2.5}$ mass on average.

The sources identified were:

- **Soil:** The first source for $PM_{10–2.5}$ was identified as originating from activities that generate crustal matter. Crustal matter is primarily composed of aluminosilicate minerals, and the source profiles extracted from receptor modelling reflect this, with Al and Si being the primary constituents and Mg, K, Ca, Ti and Fe also present. The mass ratio of Si/Al is consistently about 3:1 for both PM_{10} and $PM_{2.5}$ size fractions across all New Zealand monitoring sites and is similar to the Si/Al ratio in aluminosilicate minerals. Crustal matter (synonymous with ‘soil’ as a source reference) is predominantly a coarse particle source generated by mechanical abrasion of surface material. At urban locations, the passage of motor vehicles over roads can be the primary source of crustal-matter suspension and re-suspension (Thorpe and Harrison 2008).
- **Marine aerosol:** The second factor was identified as a marine aerosol source because of the predominance of Na and Cl, along with some Mg, S, K and Ca in similar ratios to sea water.

Further analysis of the $PM_{10–2.5}$ source contributors is provided in the following sections and compared to the data for $PM_{2.5}$ samples.

Table 3.4 Average source elemental concentration profiles for $PM_{10–2.5}$ samples from Hastings (based on 836 samples).

	Soil (ng m^{-3})	Marine Aerosol (ng m^{-3})
$PM_{10–2.5}$	1900	1400
Na	72	399
Mg	18	59
Al	70	7
Si	237	19
P	3	3
S	20	58
Cl	106	755
K	34	30
Ca	62	34
Ti	6	1
Mn	1	0
Fe	59	5
Cu	1	0
Zn	2	1

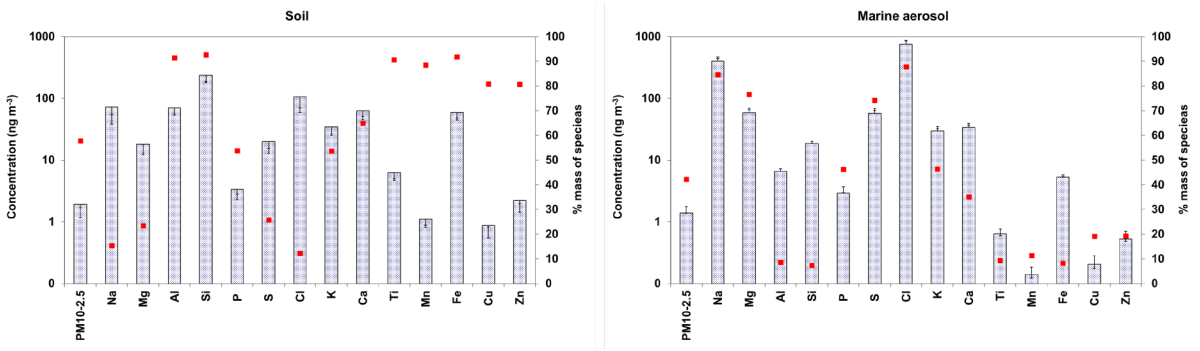

Figure 3.3 Source elemental concentration profiles for $PM_{10–2.5}$ samples from Hastings. The red dots represent the percentage of each chemical species attributed to each source.

Figure 3.4 presents the relative source contributions to $PM_{10–2.5}$ in Hastings. Also included are the 5^{th} and 95^{th} percentile confidence limits (bottom and top of error bar, respectively) in average mass contributions attributed to each of the sources, indicating the variability in average mass contributions over the monitoring period.

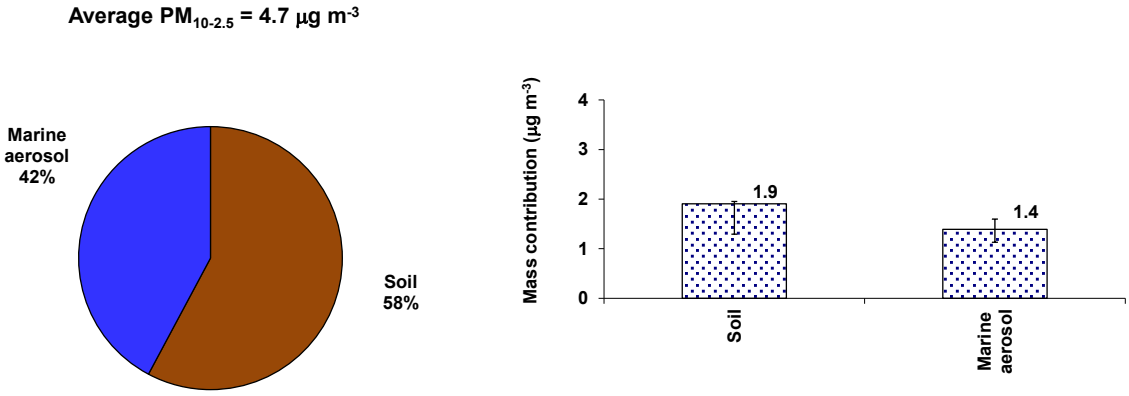

Figure 3.4 Average source mass contributions to $PM_{10–2.5}$ at Hastings over the monitoring period.

The average $PM_{10–2.5}$ source contributions over the entire monitoring period estimated from the PMF analysis showed that crustal matter (58%) was the most significant contributor to $PM_{10–2.5}$ mass, with marine aerosol contributing 42%.

3.2.3 Sources of PM_{10} at Hastings

Five source types were identified from PMF receptor modelling analysis of the Hastings PM_{10} elemental data. Table 3.5 and Figure 3.5 present the source elemental profiles and PM_{10} contributions extracted from the PMF analysis. The source contributors were found to explain 97% of the PM_{10} mass on average.

The sources identified were:

- **Biomass combustion:** As for $PM_{2.5}$, the first factor was identified as biomass combustion based on the dominance of black carbon and K in the profile. Additionally, trace amounts of As and Pb were strongly associated with the PM_{10} biomass-combustion profile.
- **Motor vehicles:** The second factor was identified as motor vehicles because of the presence of black carbon, Fe, Cu and Zn as significant elemental components. This profile is likely a combination of tail-pipe (black carbon and Zn from fuel combustion) and re-entrained road-dust emissions (Al, Si, Ca, Ti and Fe crustal-matter components, Cu from brake dust).
- **Secondary sulphate:** The third factor was identified as a secondary sulphate source because of the dominance of sulphur in the profile. This source contribution was likely to be from secondary sulphate aerosol produced in the atmosphere from gaseous precursors.
- **Marine aerosol:** The fourth factor was identified as a marine aerosol source because of the predominance of Na and Cl, along with some Mg, S, K and Ca in similar ratios to sea water.
- **Soil:** A fifth source was identified for PM_{10} as originating from activities that generate crustal matter. Crustal matter is primarily composed of aluminosilicate minerals, and the source profiles extracted from receptor modelling reflect this, with Al and Si being the primary constituents and Mg, K, Ca, Ti and Fe commonly present. The mass ratio of Si/Al is consistently about 3:1 for both PM_{10} and $PM_{2.5}$ size fractions across all New Zealand monitoring sites and is similar to the Si/Al ratio in aluminosilicate minerals. Crustal matter (synonymous with ‘soil’ as a source reference) is predominantly a coarse particle source generated by mechanical abrasion of surface material. At urban locations, the passage of motor vehicles over roads can be the primary source of crustal-matter suspension and re-suspension (Thorpe and Harrison 2008).

Further analysis of the PM_{10} source contributors is provided in the following sections and compared to the data for $PM_{2.5}$ and $PM_{10–2.5}$ samples.

Table 3.5 Average source elemental concentration profiles for PM_{10} samples from Hastings (based on 836 samples).

	Biomass Combustion (ng m^{-3})	Motor Vehicles (ng m^{-3})	Secondary Sulphate (ng m^{-3})	Marine Aerosol (ng m^{-3})	Soil (ng m^{-3})
PM_{10}	7200	1400	1300	2200	1500
Black Carbon	613	253	40	43	25
Na	8	17	27	447	57
Mg	3	7	7	65	12
Al	1	14	1	5	74
Si	2	44	3	13	250
S	10	11	45	59	14
Cl	14	44	40	852	36
K	64	21	8	29	28
Ca	5	26	4	36	46
Ti	0	2	0	0	5
Mn	0	0	0	0	1
Fe	5	22	1	4	48
Cu	1	1	0	0	0
Zn	3	4	0	0	1
As	4	1	0	0	0
Pb	1	0	0	0	0

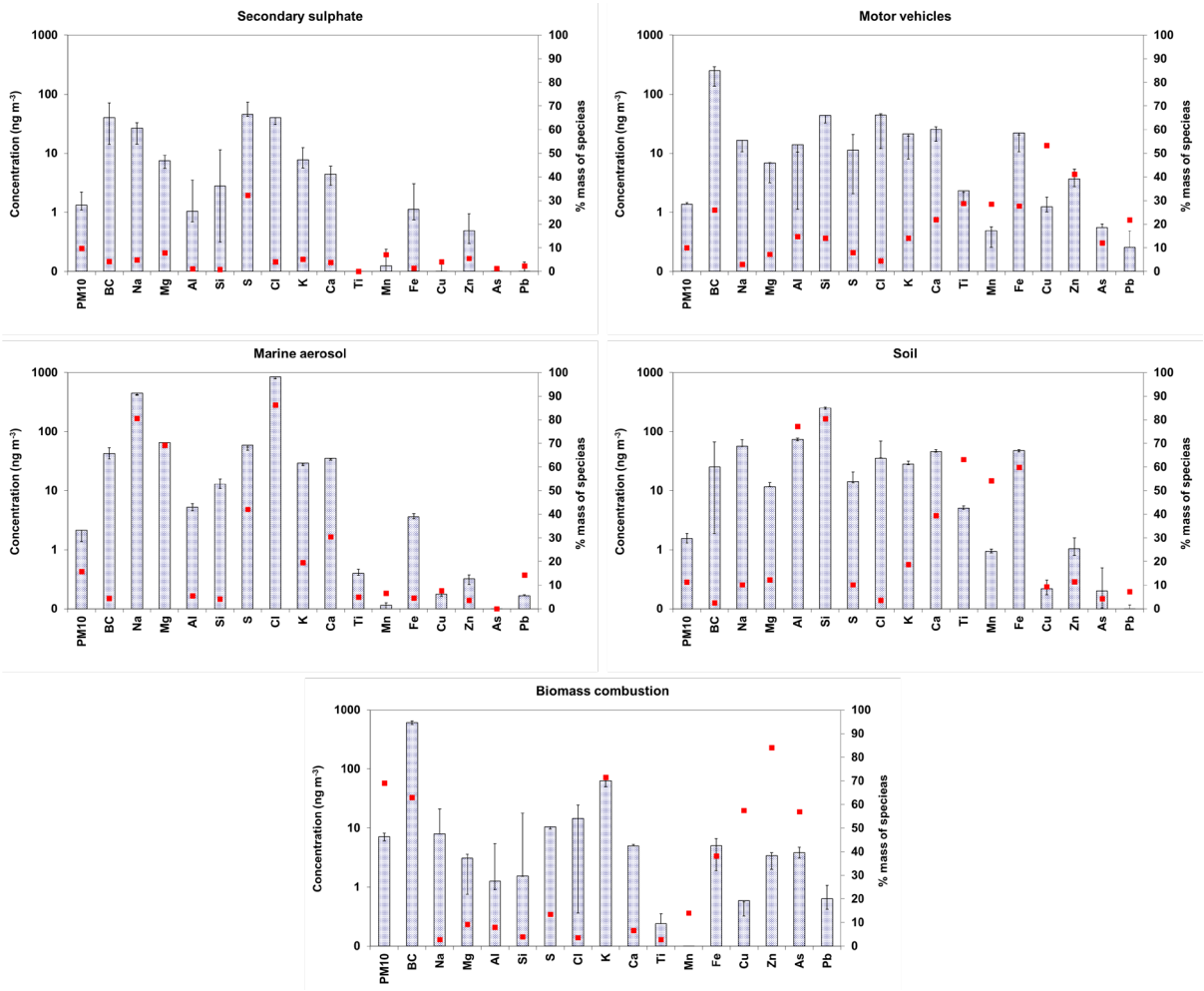

Figure 3.5 Source elemental concentration profiles for PM_{10} samples from Hastings. The red dots represent the percentage of each chemical species attributed to each source.

Figure 3.6 presents the relative source contributions to PM_{10} in Hastings. Also included are the 5th and 95th percentile confidence limits (bottom and top of error bar, respectively) in average mass contributions attributed to each of the sources, indicating the variability in average mass contributions over the monitoring period.

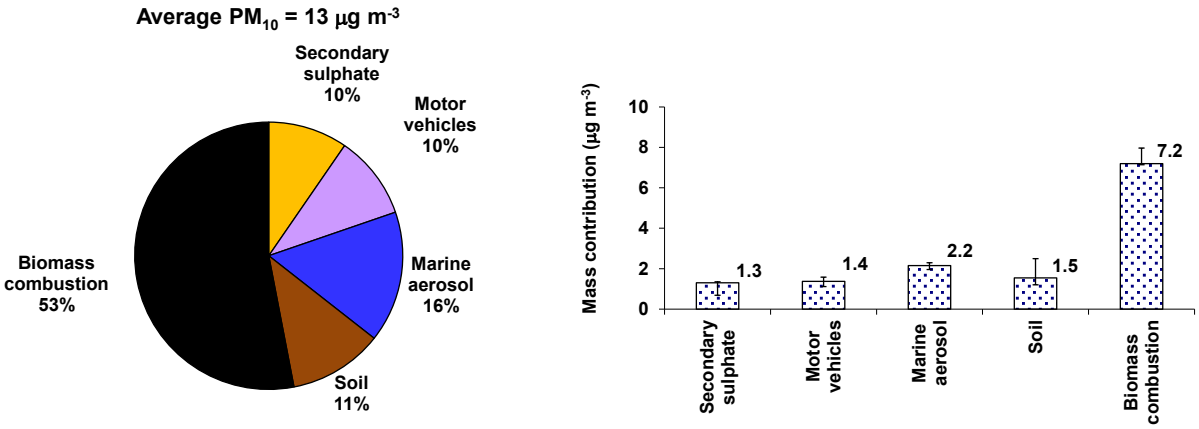

Figure 3.6 Average source mass contributions to PM_{10} at Hastings over the monitoring period.

The average PM_{10} source contributions over the entire monitoring period estimated from the PMF analysis showed that biomass combustion (53%) was the most significant contributor to PM_{10} mass, with marine aerosol (16%) the next highest, while crustal matter (11%), motor vehicles (10%) and secondary sulphate (10%) had the lowest contributions to PM_{10} mass.

3.3 Temporal Variations in Source Contributions to Particulate Matter at Hastings

Temporal variations in the source contributions to $PM_{2.5}$, $PM_{10–2.5}$ and PM_{10} at Hastings are presented in Figures 3.7, 3.8 and 3.9, respectively. It was evident from the data that airborne particulate-matter mass is dominated by biomass-combustion sources during winter, which arises primarily from emissions from solid-fuel fires used for domestic heating. During other time periods, marine aerosol, secondary sulphate and crustal-matter contributions can be significant. The motor-vehicle source contributed low levels of $PM_{2.5}$ during the monitoring period, most likely due to the local level of traffic activity near the Hastings monitoring site.

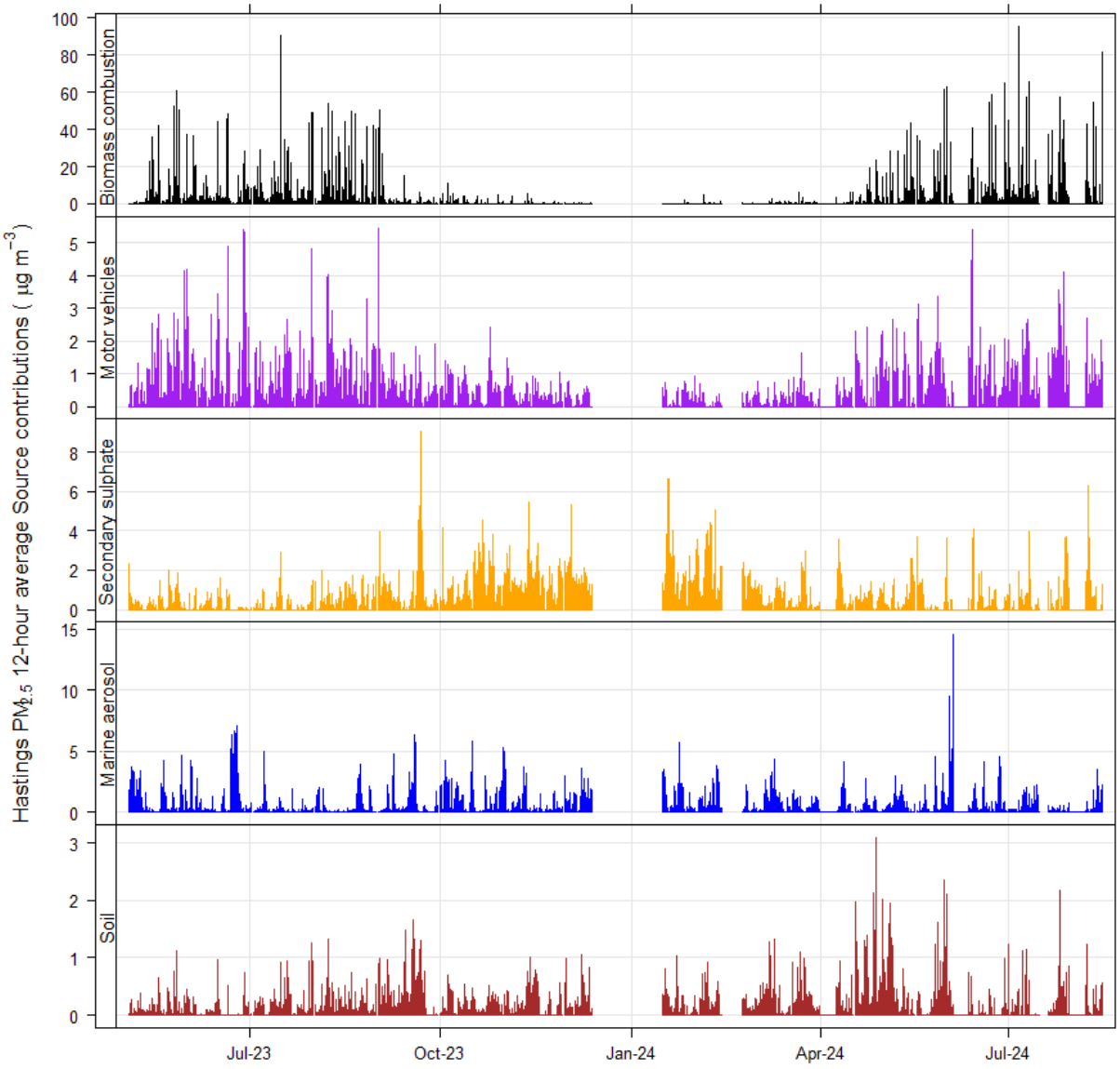

Figure 3.7 Temporal variations in relative source contributions to $PM_{2.5}$ mass (12-hour average) at the Hastings site. Gaps in the data are due to missed sampling periods.

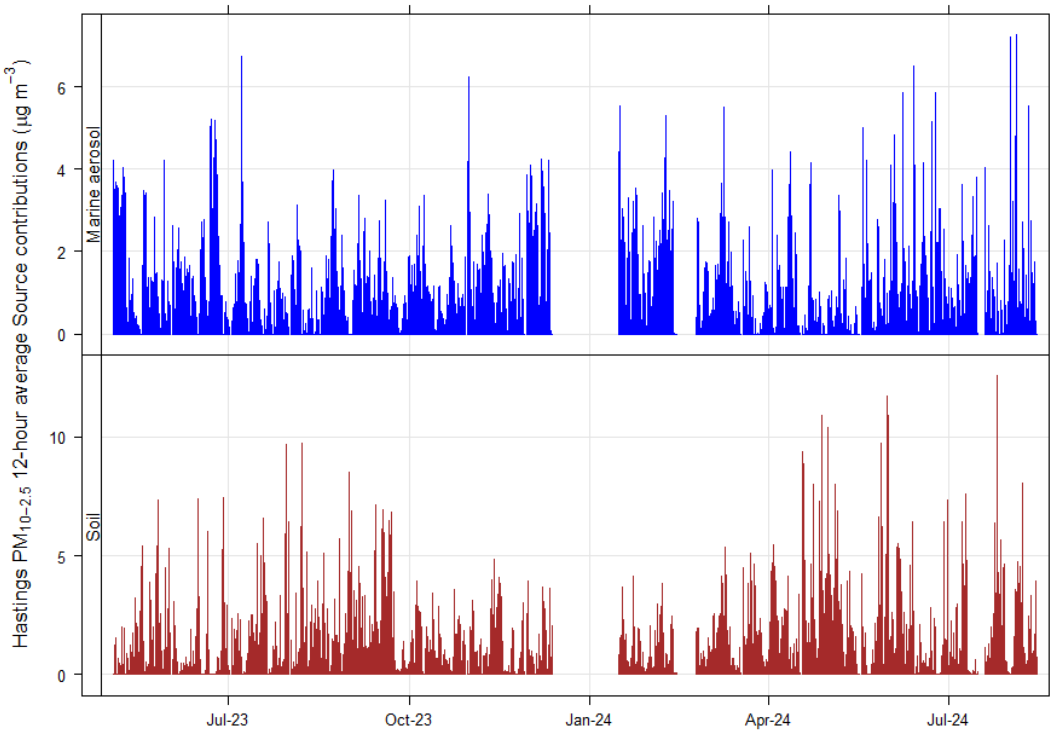

Figure 3.8 Temporal variations in relative source contributions to $PM_{10–2.5}$ mass (12-hour average) at the Hastings site. Gaps in the data are due to missed sampling periods.

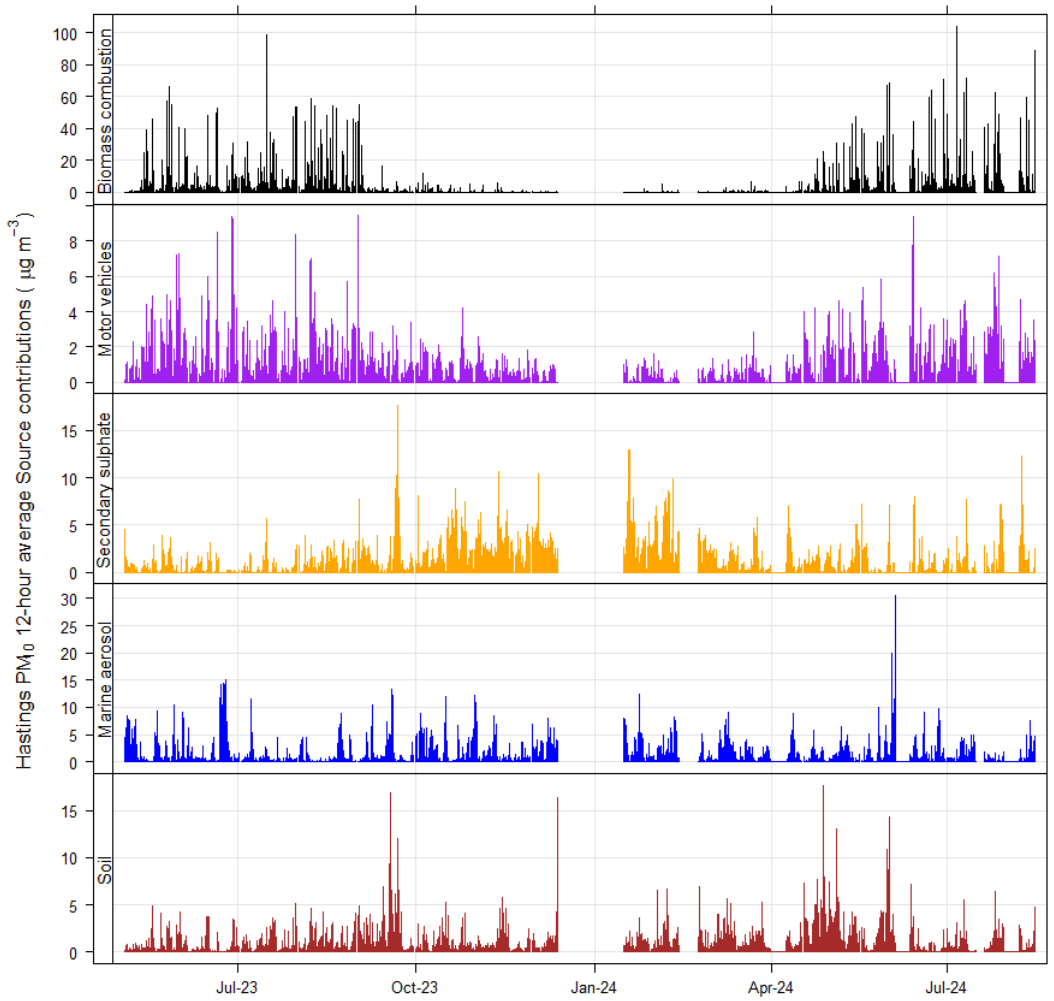

Figure 3.9 Temporal variations in relative source contributions to PM_{10} mass (12-hour average) at the Hastings site. Gaps in the data are due to missed sampling periods.

3.3.1 Seasonal and Weekday Variations in Source Contributions at Hastings

Examining the seasonal patterns in source contributions is useful for identifying sources and understanding the time of year when these may have the most impact on particulate-matter concentrations. Figure 3.10 presents the temporal variation in average monthly and average weekday source contributions to $PM_{2.5}$ and PM_{10} concentrations at the Hastings site and shows that there were distinctive patterns in concentrations for some sources. A feature of the monthly source-contribution plots presented in Figure 3.10 is the variability in day-to-day source contributions that give rise to the uncertainty in the mean estimate, as indicated by the 95th percentile confidence intervals (shaded bars on the line plots). This is likely to be the result of variable source activity coupled with meteorological influences (particulate-matter emissions from mono-directional sources will only be carried to the monitoring site when the wind is blowing in the right direction).

The dominant source of $PM_{2.5}$ and PM_{10} at Hastings was biomass combustion, which had a distinct winter peak due to the association of this source with solid-fuel fire (wood burner) emissions for domestic space heating. The motor-vehicle source was also higher during winter, most likely due to cooler winter conditions for cold-engine running and calm meteorological conditions. Secondary-sulphate particle concentrations were highest during spring and summer months likely due to the production of precursor gases by marine biota and solar forcing of atmospheric chemical reactions. The marine aerosol (sea salt) source concentrations were generally lower during winter but were likely to be primarily a meteorologically generated source (wind field strength over oceanic fetch) (Fitzgerald 1991), and peak concentrations can occur at any time of the year. As observed at a number of other locations, a peak in marine aerosol during spring (October, November) is typical for New Zealand and a result of sea-salt aerosol generated by strong equinox winds over the Southern Ocean. The crustal-matter source (soil) suggests that peak concentrations occurred during the spring and autumn months, but the aftermath of the cyclone flooding is likely to have affected crustal-matter contributions to PM_{10} at Hastings from late February 2023 onward.

The data show that the motor-vehicle source contributions to $PM_{2.5}$ and PM_{10} tended to be lower on weekends than weekdays and similarly for the soil source (statistically significant at the 95th percentile confidence intervals). The temporal variation for $PM_{2.5}$ and PM_{10} motor-vehicle and PM_{10} crustal-matter source contributions indicates that these source emissions were likely to be primarily driven by human activity, because any naturally generated emissions, such as wind-blown dust, would not show a bias for day of the week due to the random nature of meteorological events. For motor vehicles, this is likely to be indicative of lower traffic densities during the weekend than weekdays, associated with a normal working week and commercial activity. The $PM_{2.5}$ and PM_{10} soil sources may also be associated with motor vehicles as road-dust emissions but could also be due to activities such as land clearance and excavations.

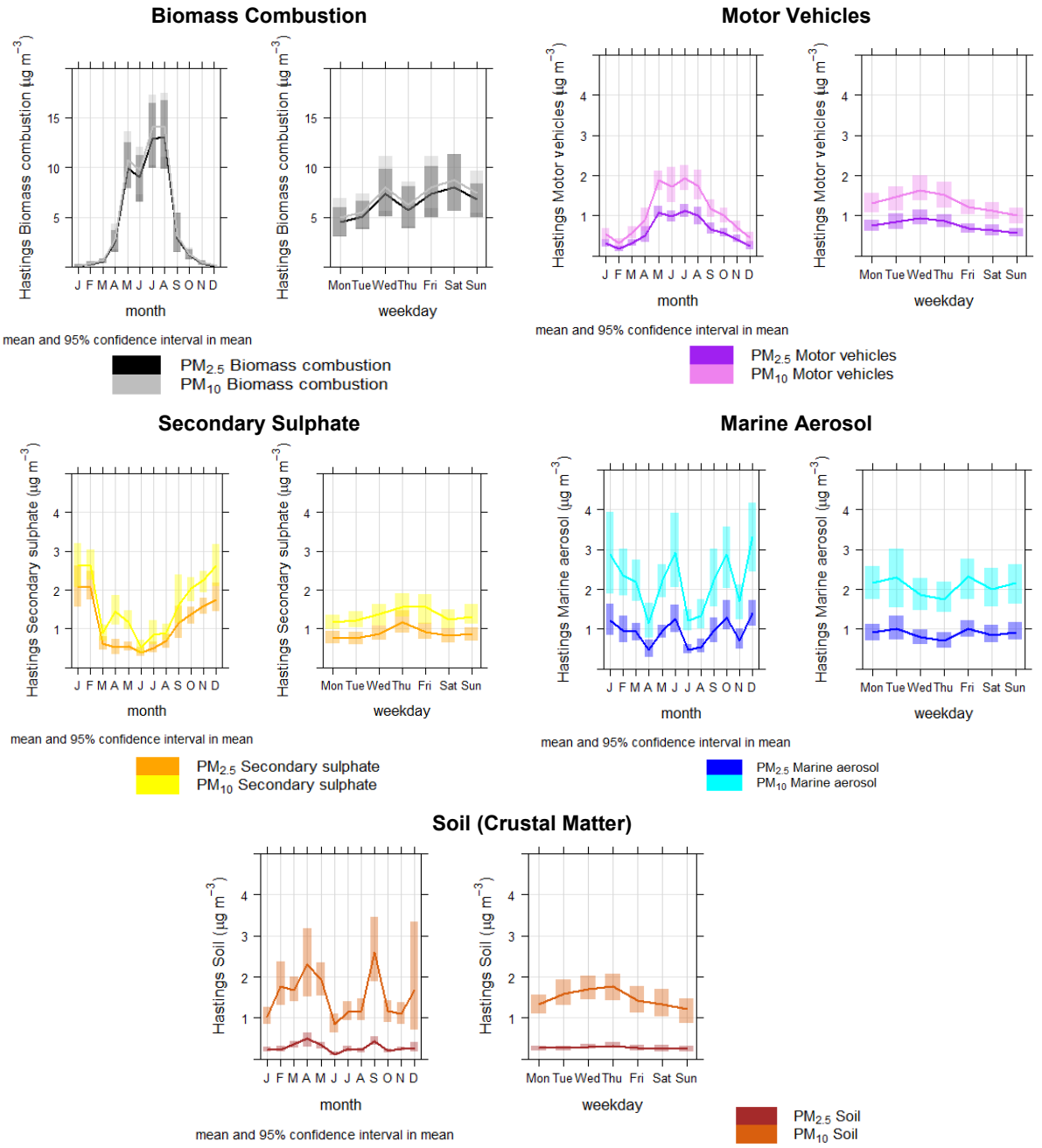

Figure 3.10 Average monthly and day-of-the-week source contributions to $PM_{2.5}$ and PM_{10} concentrations at Hastings. Shaded bars represent the 95th percentile confidence intervals in the calculated mean.

3.3.2 Diurnal Variations in Source Contributions at Hastings

The 12-hour particulate-matter sampling regime used at Hastings was based on samples collected from 6:00 pm to 6:00 am and 6:00 am to 6:00 pm, which allowed for the differentiation of source contributions during day- and night-time periods. The data shows that the highest concentrations captured on the overnight samples (18:00–06:00) were from biomass combustion sources on winter nights for both $PM_{2.5}$ and PM_{10} (Figures 3.11 and 3.12, respectively). Winter nights, along with autumn and spring nights, were substantially higher than the respective biomass combustion source contributions to daytime samples for the same time periods.

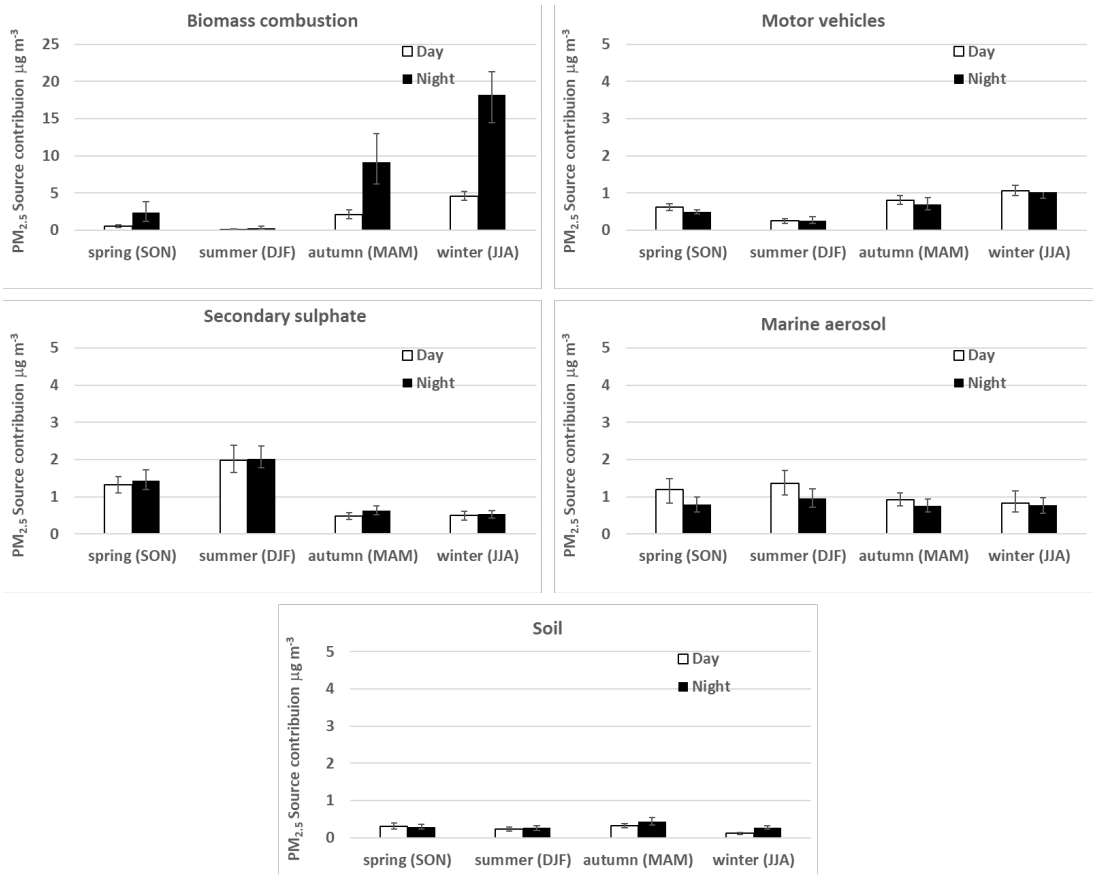

Figure 3.11 Average day- and night-time source contributions during different seasons to $PM_{2.5}$ concentrations at Hastings. Error bars represent the 95th percentile confidence intervals in the calculated mean.

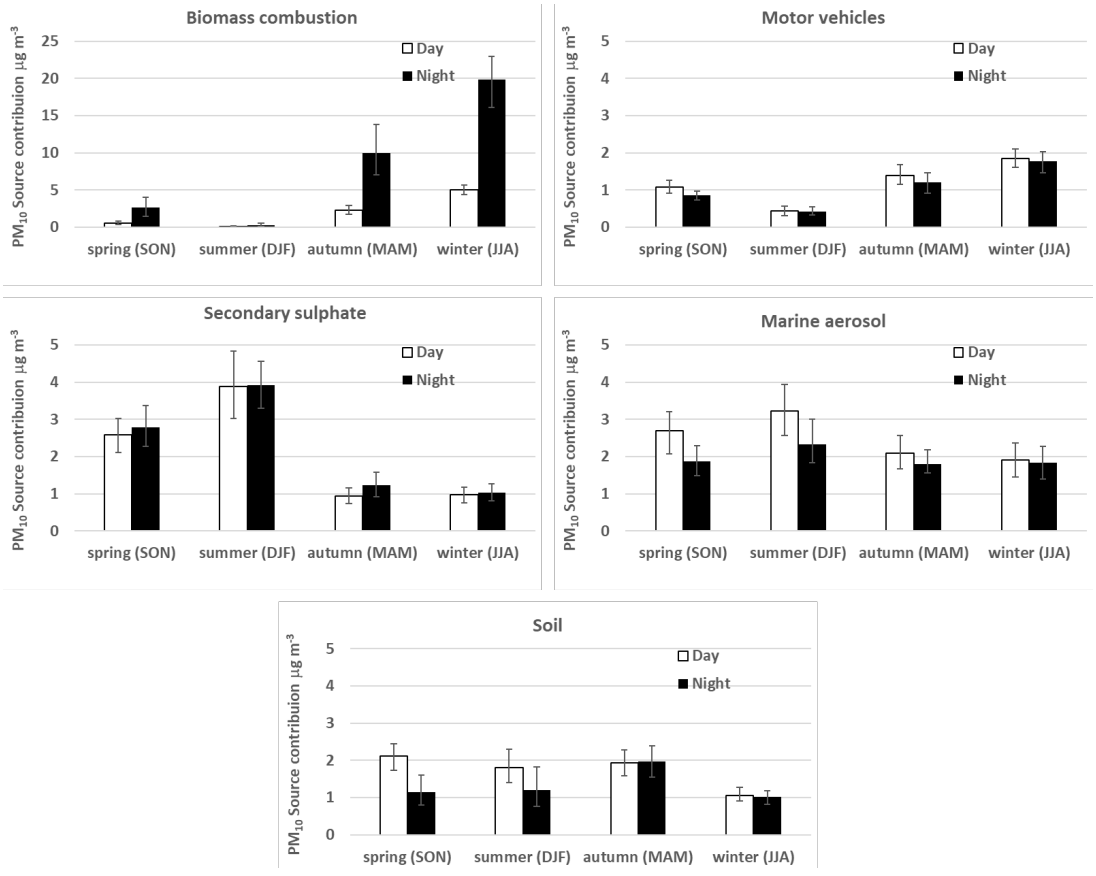

Figure 3.12 Average day- and night-time source contributions during different seasons to PM_{10} concentrations at Hastings. Error bars represent the 95th percentile confidence intervals in the calculated mean.

Daytime contributions to $PM_{2.5}$ and PM_{10} were slightly higher for motor-vehicle sources, likely reflecting higher traffic volumes during daylight hours, although the differences were not statistically significant at the 95 percentile confidence intervals. Similarly, there was no distinct diurnal pattern evident for secondary sulphate and marine aerosol sources in any season, nor for crustal-matter sources during summer, autumn and winter. However, for crustal matter, there was a significant diurnal difference in concentrations during spring months with average daytime concentrations double the night-time average concentration, and this likely reflects a combination of activities that generate dusts and stronger winds carrying the crustal-matter particles to the monitoring site. The analysis of source contributions with wind direction presented in Section 3.4 (see Figure 3.17) suggests that during spring (September–November 2023), peak crustal-matter concentrations arrived at the site from the west under higher wind speeds.

3.4 Variations in Source Contributions at Hastings with Wind Direction

Bivariate polar plots using the source contributions to $PM_{2.5}$ and PM_{10} were produced using R statistical software and the *openair* package (Carslaw 2012; Carslaw and Ropkins 2012; R Core Team 2015). Using bivariate polar plots, source contributions can be shown as a function of both wind speed and direction, providing invaluable information about potential source regions and how pollution from a specific source builds up. To produce the polar plots, wind speeds and directions were vector-averaged using functions available in *openair*. A full description of the vector-averaging process can be found in Carslaw (2012). The conditional probability function statistic ‘cpf’ has been used here, as described in Section 2.2.1. Because of the smoothing involved, the colour scale used in the plots is only to provide an indication of overall pattern and should not be interpreted in concentration units. The meteorological data used for the polar-plot analysis was that supplied by Hawke’s Bay Regional Council from the Hastings (St John’s College) monitoring site.

3.4.1 Biomass Combustion

Biomass-combustion source contributions to $PM_{2.5}$ and PM_{10} were considered to be primarily from domestic solid-fuel fire emissions. Figure 3.13 presents a bivariate polar plot of biomass-combustion contributions to $PM_{2.5}$. Figure 3.13 shows that peak biomass combustion contributions occurred under light winds (less than 5 m/s) from the south to southwest. This suggests that light southerly winds under cold and calm anti-cyclonic synoptic meteorological conditions, coupled with domestic fire emissions and poor dispersion, were likely responsible for elevated particulate-matter concentrations at Hastings, similar to other New Zealand urban locations (Trompetter et al. 2010; Ancelet et al. 2012; Grange et al. 2013; Ancelet et al. 2014b).

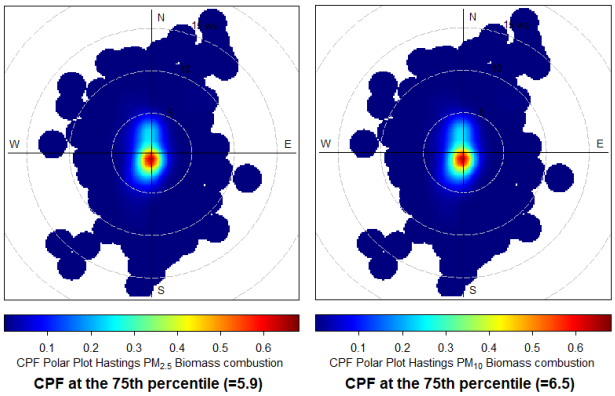

Figure 3.13 Polar plot of biomass-combustion contributions to $PM_{2.5}$ (left) and PM_{10} (right) concentrations. The radial dimensions indicate wind speed in 5 m s^{-1} increments, and the colour contours indicate the relative contribution to each wind direction / speed bin. Because of the smoothing involved, the colour scale used in the plots is only to provide an indication of overall pattern and should not be interpreted in concentration units.

3.4.2 Motor Vehicles

Peak motor-vehicle contributions at the monitoring site occurred under winds from the northwest and southwest quadrants (Figure 3.14). This is likely to represent the contribution from motor vehicles on the local roading network and activity in the commercial centre to the west of the monitoring site. When wind direction aligns with the centreline of roadways, the road acts as a line source, and this will convey the highest concentrations of motor-vehicle emissions.

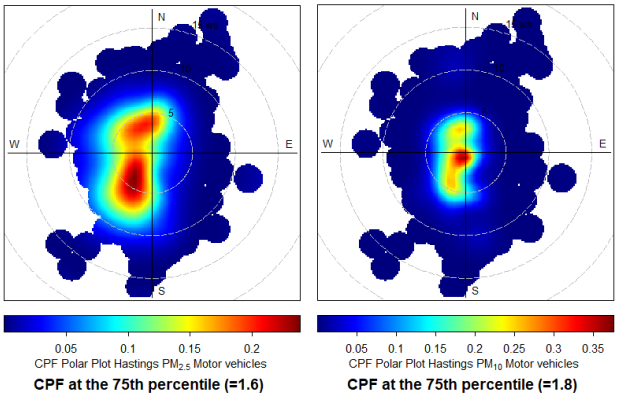

Figure 3.14 Polar plot of motor-vehicle contributions to $PM_{2.5}$ (left) and PM_{10} (right) concentrations The radial dimensions indicate wind speed in 5 m s^{-1} increments, and the colour contours indicate the relative contribution to each wind direction / speed bin. Because of the smoothing involved, the colour scale used in the plots is only to provide an indication of overall pattern and should not be interpreted in concentration units.

3.4.3 Secondary Sulphate

Peak secondary-sulphate contributions at Hastings originated from northwest of the monitoring site (Figure 3.15). Sources of secondary-sulphate precursor gases include anthropogenic emissions, such as combustion of sulphur-containing fuels and industrial emissions, or natural sources, including oceanic (e.g. dimethyl sulphide produced by marine phytoplankton) and volcanic and geothermal activity (SO_2 and H_2S). In a recent study, it was shown that emissions of precursor sulphur gases from the Taupō Volcanic Zone have a significant influence on regional secondary-sulphate concentrations (Davy et al. 2024).

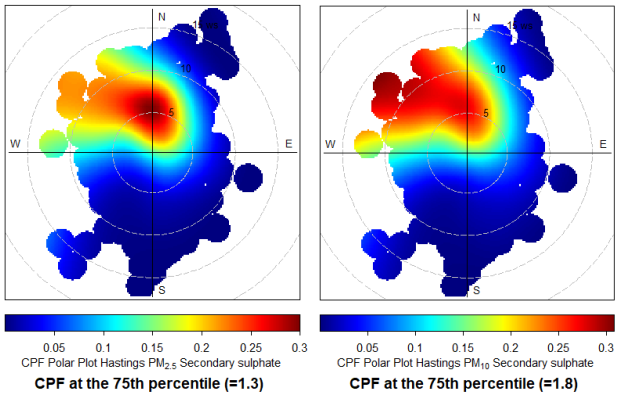

Figure 3.15 Polar plot of secondary-sulphate contributions to $PM_{2.5}$ (left) and PM_{10} (right) concentrations. The radial dimensions indicate wind speed in 5 m s^{-1} increments, and the colour contours indicate the relative contribution to each wind direction / speed bin. Because of the smoothing involved, the colour scale used in the plots is only to provide an indication of overall pattern and should not be interpreted in concentration units.

3.4.4 Marine Aerosol

Marine aerosol contributions in Hastings peaked under higher wind speeds from the northerly and easterly sectors (Figure 3.16). The most likely source of marine aerosol was Hawke Bay and the Pacific Ocean.

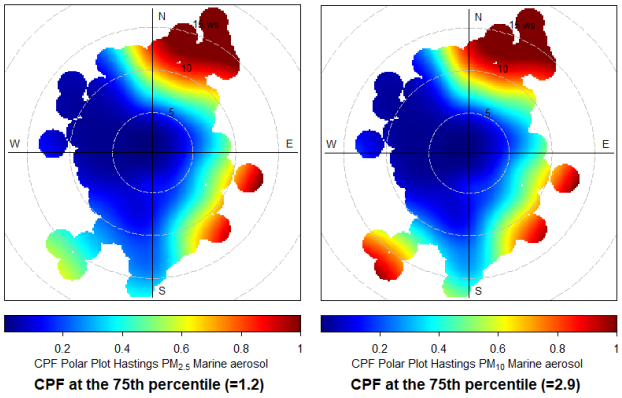

Figure 3.16 Polar plot of marine-aerosol contributions to $PM_{2.5}$ (left) and PM_{10} (right) concentrations. The radial dimensions indicate wind speed in 5 m s^{-1} increments, and the colour contours indicate the relative contribution to each wind direction / speed bin. Because of the smoothing involved, the colour scale used in the plots is only to provide an indication of overall pattern and should not be interpreted in concentration units.

3.4.5 Soil

Figure 3.17 shows that the $PM_{2.5}$ crustal-matter contributions peaked in stronger (>10 m/s) NW–SW winds. Interestingly, such wind speeds (> 36 km/hr) have been estimated as the threshold for wind-action/uplift of dusts in urban areas (Banari et al. 2023). The crustal matter in urban areas is likely to be generated by a combination of vehicle dusts from road surfaces, unsealed yards or other dust-generating activities. In addition, agricultural activities; land excavations; and the processing, handling or storage of bulk aggregate may also be potential sources. However, the peak crustal-matter concentrations observed for the Hastings site may be associated with dusts generated in the aftermath of Cyclone Gabrielle flooding. Further discussion on the impact of Cyclone Gabrielle on particulate-matter concentrations at Hastings are provided in Section 4.3.

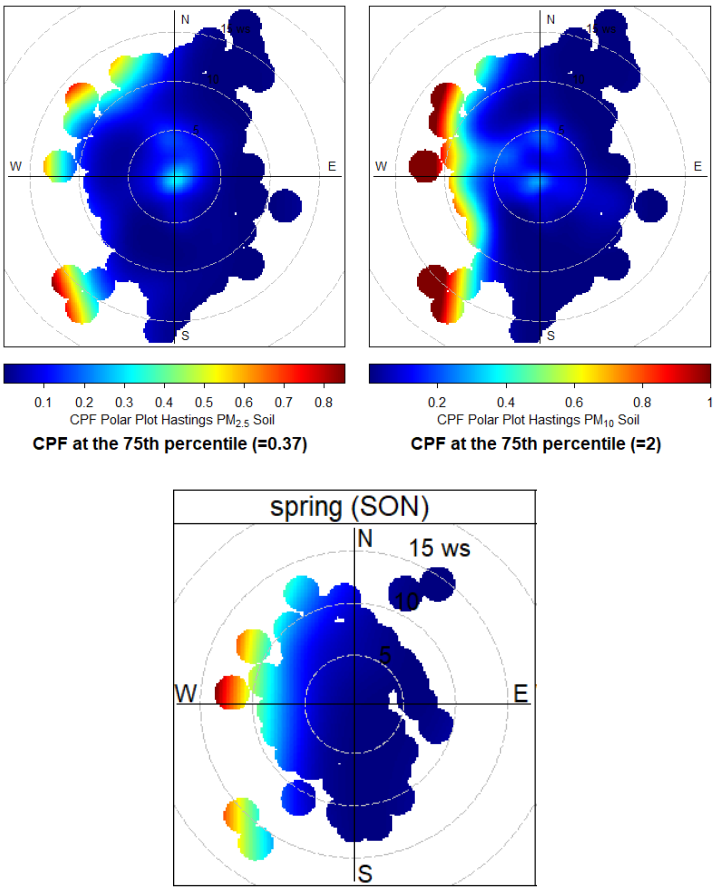

Figure 3.17 Polar plot of soil contributions to $PM_{2.5}$ (top left) and PM_{10} (top right) concentrations, along with the contributions during spring (bottom). The radial dimensions indicate wind speed in 5 m s^{-1} increments, and the colour contours indicate the relative contribution to each wind direction / speed bin. Because of the smoothing involved, the colour scale used in the plots is only to provide an indication of overall pattern and should not be interpreted in concentration units.

4.0 DISCUSSION OF THE HASTINGS RECEPTOR-MODELLING RESULTS

Analysis of $PM_{2.5}$ and $PM_{10–2.5}$ filter-based sample sets of air particulate matter in Hastings showed that peak concentrations occurred during winter. Five source types from receptor modelling of sample composition were identified as the primary contributors to $PM_{2.5}$ and PM_{10} at Hastings. The receptor-modelling analysis showed that some source contributors had distinct seasonality and that the peak winter particulate-matter concentrations were primarily influenced by biomass-combustion sources. The simultaneous collection of $PM_{2.5}$ and $PM_{10–2.5}$ at the Hastings monitoring site has provided the means to intercompare source contributions to each size fraction and examine any differences.

4.1 Sources of Particulate Matter at Hastings

4.1.1 Biomass Combustion

Analysis of temporal and seasonal patterns showed that particulate matter from biomass combustion peaked during the winter, contributed the highest concentrations during the night and showed no significant variation between days of the week (Figure 3.10). The lack of variation between days of the week was not surprising, as peak biomass-combustion contributions occur under meteorological conditions conducive to the build-up of pollutants (cold and calm, anti-cyclonic conditions), which could occur on any day of the week. The biomass-combustion source was most likely to have originated from domestic wood combustion for home heating and included traces of As and Pb in the source chemical profile, suggesting that CCA-treated wood and old painted timber were being used as fuel. The use of such contaminated timber as fuel for domestic fires is common throughout New Zealand (Davy et al. 2012; Ancelet et al. 2013a; Mitchell et al. 2013; Ancelet et al. 2014a, 2014b; Davy et al. 2014, 2016; Davy and Trompetter 2017a, 2017b, 2018, 2020).

4.1.2 Motor Vehicles

The motor-vehicle source was identified as a minor contributor to $PM_{2.5}$ (8%) and PM_{10} (10%). As indicated in the previous sections, the motor-vehicle source is likely to be a combination of vehicular tail-pipe emissions (fine particles) and re-suspended soil (coarse particles) generated by the turbulent passage of vehicles on roads, car-parking areas and unsealed yards. Further support for the anthropogenic origin of the motor-vehicle source was that weekday contributions were higher than for weekends (see Figure 3.10), indicating an association with anthropogenic activity (traffic density and associated weekday commuter and commercial activities).

4.1.3 Secondary Sulphate

Analysis of the sulphate source contributions using bivariate polar plots (Figure 3.15) showed that peak contributions from secondary sulphate were transported from northwest of the sampling site. Significant sources of secondary sulphate include combustion emissions from high-sulphur fuels (e.g. coal, or ships using residual fuel oil), industrial emissions of precursor gases, marine phytoplankton activity (release of dimethyl sulphide as a gaseous precursor) and volcanic emissions (Davy et al. 2024). The atmospheric reaction pathway for these gases is similar no matter the source, and, ultimately, the sulphate aerosol has a similar chemical signature that is resolved as a single source by factor-analysis techniques such as PMF. Analysis of data from around New Zealand indicates that the secondary-sulphate source is largely of natural origins, unless monitoring is near ports or point-source emissions, such as coal burning and industrial processes (e.g. fertiliser production) (Davy et al. 2024). Note that

the conversion of precursor gases to sulphate particles can take from hours to days depending on atmospheric conditions (temperature, relative humidity, solar insolation) and the presence (or absence) of other reactive species (Seinfeld and Pandis 2006). The higher concentrations during summer are likely due to the influence of solar forcing of atmospheric chemistry and seasonal cycles in natural source (marine phytoplankton) production.

Secondary sulphate is primarily a fine particle due to the gas-to-particle formation reaction process, but some of the sulphate particle size range does extend into the coarse fraction (Anlauf et al. 2006), particularly where heterogeneous atmospheric chemistry takes place on the surface of particles (such as marine aerosol) or in aerosol droplets during the reaction of sulphur gaseous species to form secondary sulphate particle species (Gard et al. 1998; O'Dowd et al. 2000; George and Abbatt 2010). The secondary-sulphate source chemical profiles for the Hastings samples (Tables 3.3 and 3.4) indicate that sea-salt elements (Na, Mg, K, Ca) are also associated with the sulphur, suggesting heterogenous sulphate particle formation reactions with marine aerosol. Similar results for higher PM_{10} secondary sulphate concentrations compared to $PM_{2.5}$ have been observed for Auckland datasets (Davy et al. 2017).

4.1.4 Marine Aerosol

Marine aerosol was found to be a significant contributor to $PM_{2.5}$ (10%), and more so for PM_{10} (15%), in Hastings and is generally a significant particle source in New Zealand airsheds due to the isolated oceanic location of the landmass. The elemental composition for the marine-aerosol source closely resembles that of seawater (Lide 1992), and the source profile is therefore dominated by chlorine and sodium. Analysis of temporal and seasonal variations in marine aerosol showed higher concentrations during spring and summer. However, marine aerosol concentrations could also peak at other times, as the generation of marine aerosol is dependent on meteorological factors, such as wind speeds across an oceanic fetch and evaporation potential. The data indicates that there was significantly less sea salt present in the local atmosphere for the 2023–2024 monitoring period than for 2022–2023. This was likely to be primarily driven by variations in synoptic weather and Southern Hemisphere circulation patterns. Analysis of peak marine-aerosol contributions to particulate-matter concentrations (Figure 3.16) showed distinct northeast and southeasterly directionality during higher wind speeds at Hastings, which was consistent with the most significant oceanic wind directions.

4.1.5 Soil

The chemical composition profile for the soil source contains Al and Si as major constituents, with these elemental ratios typical of crustal-matter minerals. The soil source CPF analysis (Figure 3.17) demonstrated a strong westerly directionality, with the top 25% of concentrations arriving at windspeeds greater than 10 m/s (36 km/hr) for both $PM_{2.5}$ and PM_{10}. The analysis of temporal variations for the soil source showed that peak concentrations occurred during March 2023 immediately after the flooding caused by Cyclone Gabrielle (Davy and Trompetter 2023), and then again in autumn of 2024. Analysis of temporal patterns shows that there was a tendency for higher concentrations to occur on weekdays compared to weekends, signifying that the source was likely due to anthropogenic activity. This suggests that the soil source was likely associated with human activities that generated the dusts, which were then dispersed by stronger winds.

4.2 Analysis of Contributions to Particulate Matter on Peak Days

For air-quality management purposes and the protection of human health, contributions from various emission sources to peak particulate-matter concentration events are of most interest. The Streaker sampler system was run on a 06:00–18:00 and 18:00–06:00 12-hourly sampling regime to capture the day- and night-time diurnal patterns observed in particulate-matter mass concentration data. Therefore, the 24-hour average generated from the resulting source-apportionment data was not midnight to midnight (as used by NESAQ) but rather 6:00 am to 6:00 am, and, as a consequence, the 24-average will be numerically different. However, the data will be indicative of those sources that are dominating peak particulate-matter concentrations as measured at the site and are still useful for air-quality management purposes. Note that the sampling period includes two winters.

Of the days when samples were collected during the monitoring period, there were 92 days (all during winter) when $PM_{2.5}$ concentrations were higher than 15 µg m^{-3}, the WHO AAQG for $PM_{2.5}$. The relative source contributions to $PM_{2.5}$ on those peak days are presented in Figure 4.1.

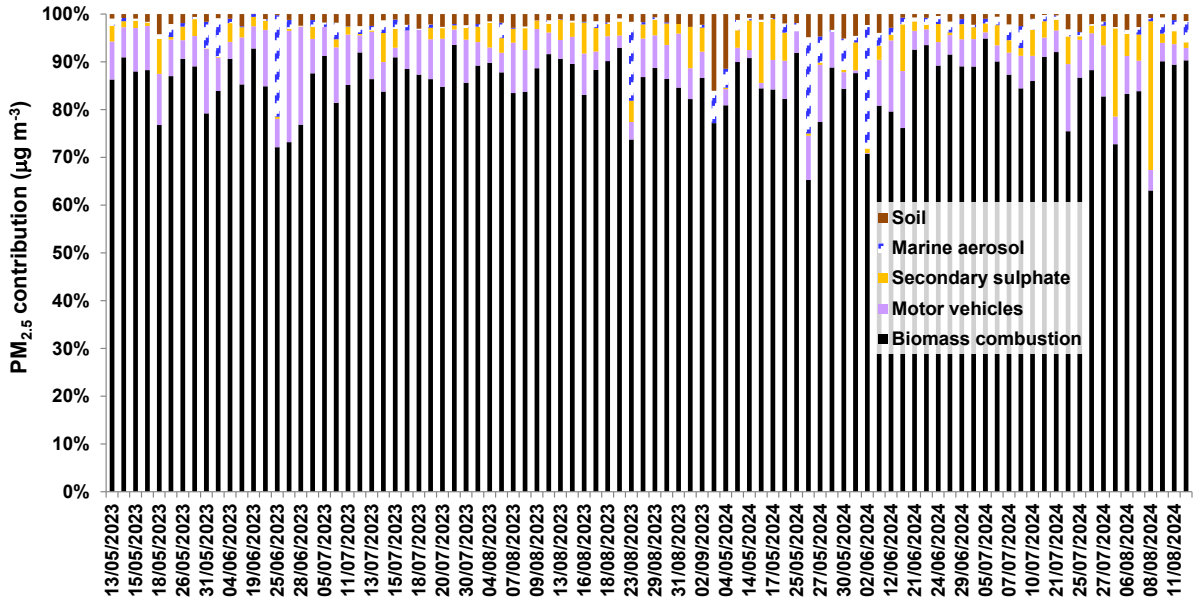

Figure 4.1 Source mass contributions to peak $PM_{2.5}$ events (>15 µg m^{-3}) at Hastings.

During peak winter $PM_{2.5}$ concentrations, contributions from biomass combustion sources were responsible for 80% of $PM_{2.5}$ mass, while particles from other emission sources were generally low, including any contribution from natural sources (marine aerosol and secondary sulphate).

Peak concentration days for PM_{10} were those days with concentrations above 33 µgm^{-3} (the 'Alert' category, as described in Table 2.1). There were thirty-nine sampling days during the monitoring campaign where PM_{10} exceeded the Alert category, as presented in Figure 4.2.

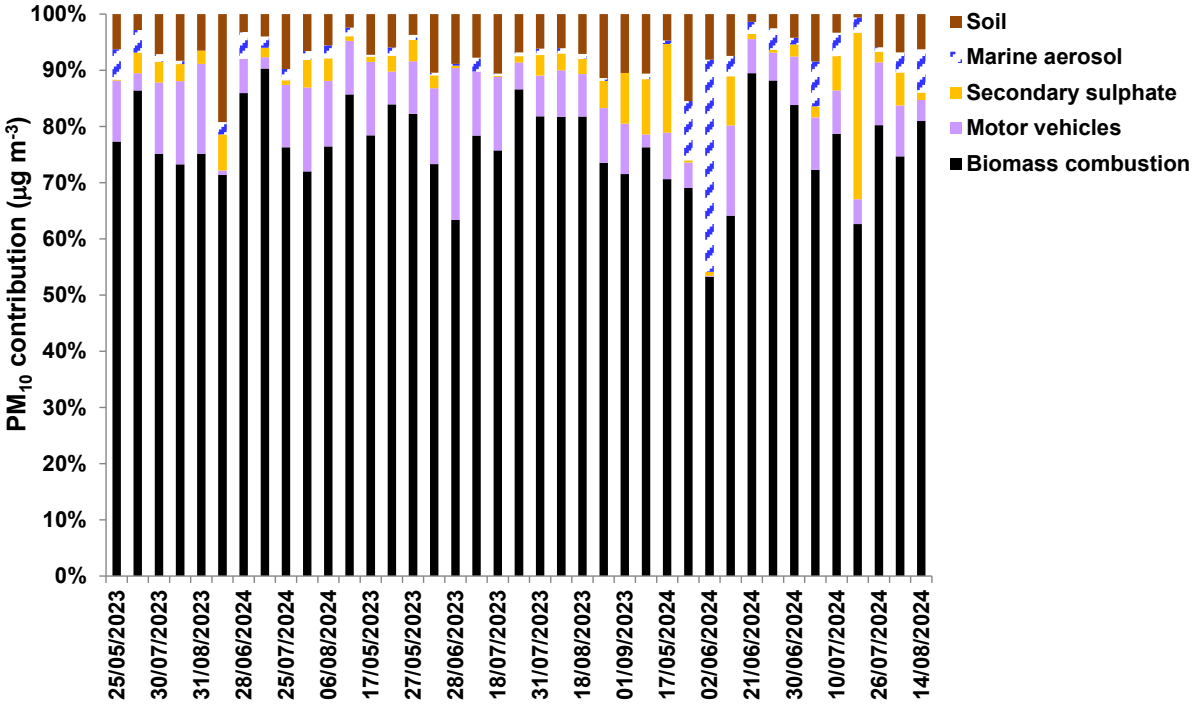

Figure 4.2 Source mass contributions to peak PM_{10} events (>50 µg m^{-3}) at Hastings.

Figure 4.2 shows that biomass combustion was responsible for an average of 70% of PM_{10} mass on high particulate-matter concentration days during winter. The result is consistent with the location of the Hastings monitoring site in a residential area, where solid-fuel fires are used for home heating during winter. In New Zealand urban areas, high particulate-matter events are generally dominated by biomass-combustion emissions during winter. Concentrations generally peak in the late evening, and most (>80%) of the particulate matter is in the $PM_{2.5}$ fraction (Davy et al. 2012; Ancelet et al. 2014c, 2015; Davy et al. 2016, 2017; Davy and Trompetter 2020).

4.3 Comparison of Hastings Particulate-Matter Composition and Source Contributions Before and After Cyclone Gabrielle

Sampling of $PM_{2.5}$ and PM_{10} (May 2022 – April 2023) followed by compositional analysis and receptor modelling was previously undertaken for Hastings (Davy and Trompetter 2023) using two NESAQ-compliant gravimetric samplers (MetOne E-SEQ-FRM sequential USEPA reference method particulate sampler). With the advent of Cyclone Gabrielle and the clean-up of silt from the flooding, it was recognised that this may have an impact on air quality in the airshed. Therefore, particulate matter ($PM_{2.5}$ and $PM_{10–2.5}$) sampling and compositional measurements were continued at Hastings using the Streaker sampling system, as this provided the opportunity for cost-effective and higher time-resolution continuous monitoring.

While noting that there can be considerable variation in emissions and meteorology year-to-year that will impact the composition of atmospheric particles and the contributions of emission sources to total particulate-matter concentrations, the average contributions are likely to reflect the relative impact of sources at the time that monitoring was undertaken. When comparing the ‘before and after’ Cyclone Gabrielle particulate-matter composition, the data has been partitioned such that ‘before’ the impact of the cyclone was any data up to mid-February 2023, when the cyclone struck, and ‘after’ was all data for the year after (April 2023 – May 2024, i.e. excluding the 2024 winter) that was likely to contain information for any differences in relative contributions.

Figure 4.3 presents a comparison of the source contributions for $PM_{2.5}$ and PM_{10} before and after Cyclone Gabrielle.

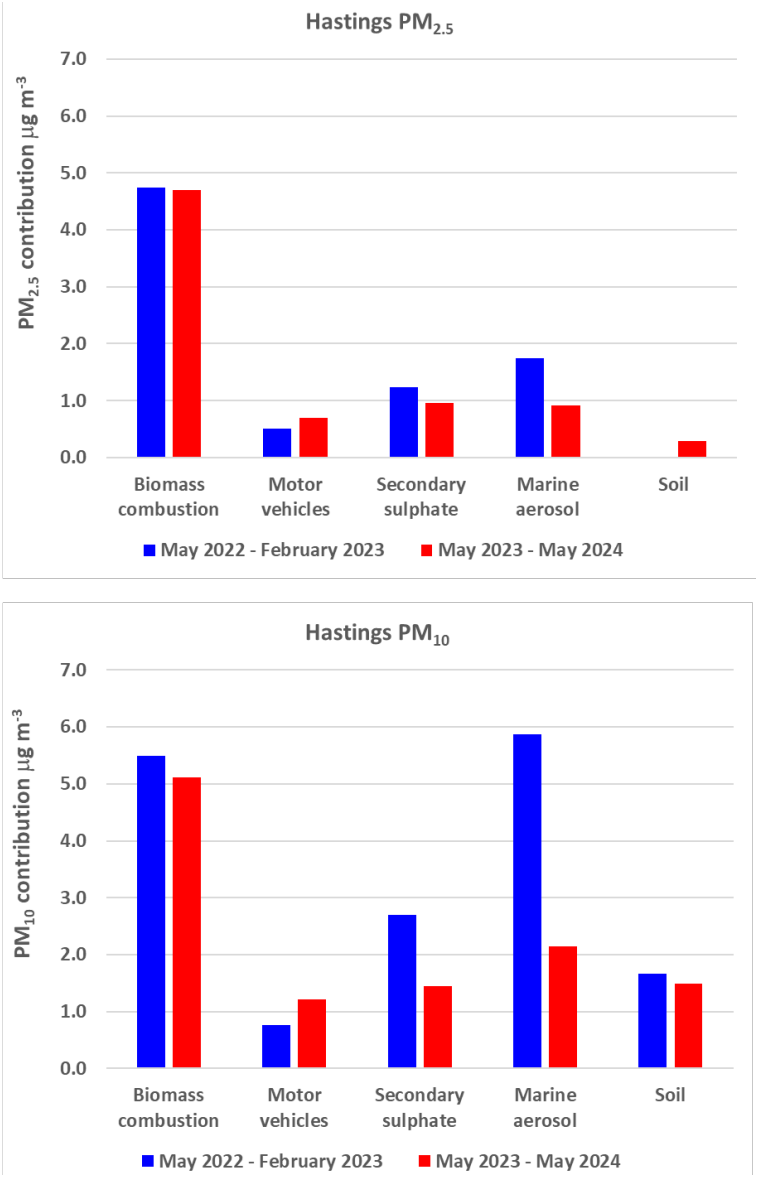

Figure 4.3 Source mass contributions to $PM_{2.5}$ (top) and PM_{10} (bottom) at Hastings for before (blue) and after (red) the impact of Cyclone Gabrielle.

The data shows that there was an increase in motor-vehicle contributions for both $PM_{2.5}$ and PM_{10} post-Cyclone Gabrielle and that a crustal-matter source was resolved for $PM_{2.5}$. The underlying compositional data indicates that $PM_{2.5}$ crustal-matter components (Al, Si, Ca, Ti and Fe) were present in particulate matter at about twice the concentration post-cyclone than pre-cyclone. The results suggest that there was an increase of approximately 0.5 µg m^{-3} in $PM_{2.5}$ crustal-matter particles, both as motor-vehicle-associated road dust and wind-blown soil post-cyclone as measured at the Hastings monitoring site. Conversely, there was a significant decrease (approximately 50%) in both marine- and secondary-sulphate aerosol contributions, representing an approximate decrease of 1 µg m^{-3} for $PM_{2.5}$ and 4 µg m^{-3} for PM_{10} post-cyclone. Both the marine aerosol and secondary sulphate are primarily natural sources of particulate matter and the variations from year to year likely to be driven by synoptic weather patterns for marine aerosol and oceanic phytoplankton activity in the case of secondary sulphate concentrations (Davy et al. 2024). Biomass-combustion contributions were relatively similar for the two time periods (i.e. winter 2022 and winter 2023).

5.0 SUMMARY OF HASTINGS PARTICULATE-MATTER COMPOSITION AND SOURCE CONTRIBUTIONS

A 15-month-long (May 2023 to August 2023) $PM_{2.5}$ and $PM_{10–2.5}$ airborne-particle sampling programme at Hastings formed the basis of a study of particulate-matter compositional analysis and the attribution of sources contributing to particulate-matter concentrations. The work also served to examine the relative impact on sources of particulate-matter in the Hastings airshed after the impacts of Cyclone Gabrielle.

Five main source types were extracted from the data by receptor-modelling techniques; these sources of particulate matter were biomass combustion, motor vehicles, secondary sulphate, marine aerosol and soil. The primary source of peak winter $PM_{2.5}$ in Hastings was the biomass-combustion source, which was attributed to the use of solid-fuel fires for home heating and contributed 80% of the total $PM_{2.5}$ mass during peak concentrations (>15 μg m^{-3}). Contributions to peak PM_{10} concentrations reflected the influence of $PM_{2.5}$ combustion sources, along with a greater influence of coarse-particle sea salt and crustal matter. The biomass-combustion source was found to be contaminated with As and Pb due to the use of CCA-treated timber and old painted timber, respectively, as fuel.

When the data was compared to the 2022–2023 $PM_{2.5}$ and PM_{10} monitoring campaign (Davy and Trompetter 2023), it shows that there was an increase in motor-vehicle contributions for both $PM_{2.5}$ and PM_{10} post-Cyclone Gabrielle and a significant increase in crustal-matter contributions to $PM_{2.5}$. The results suggest that there was an increase of approximately 0.5 μg m^{-3} in $PM_{2.5}$ crustal-matter particles, both as motor-vehicle-associated road dust and wind-blown soil post-cyclone as measured at the Hastings monitoring site. Biomass-combustion contributions were relatively similar for the two time periods (i.e. winter 2022 and winter 2023). Conversely, there was a significant decrease (approximately 50%) in both in marine- and secondary-sulphate aerosol contributions representing an approximate decrease of 1 μg m^{-3} for $PM_{2.5}$ and 4 μg m^{-3} for PM_{10} post-cyclone. The decrease in marine- and secondary-sulphate aerosol post-cyclone is likely to be related to differences in synoptic meteorological conditions and atmospheric circulation patterns between the time periods.

While the results from the monitoring indicate that crustal matter ‘dust’ events resulting in high airborne particulate-matter concentrations (i.e. close to the $PM_{2.5}$ World Health Organization Guideline or the PM_{10} National Environmental Standard) were not captured at the monitoring site in the wake of the Cyclone Gabrielle aftermath, localised dust nuisance may have occurred elsewhere in the airshed, particularly around activities that involved soil disturbance. Soil particles, being relatively large and heavy, are likely to settle out of the atmosphere rapidly downwind of a re-suspension source unless there are significant wind speeds at the same time to carry finer particles further afield.

6.0 ACKNOWLEDGEMENTS

The authors thank Chris Purcell for filter analytical measurements and accelerator maintenance.

7.0 REFERENCES

Allen JO, Mayo PR, Hughes LS, Salmon LG, Cass GR. 2001. Emissions of size-segregated aerosols from on-road vehicles in the Caldecott Tunnel. *Environmental Science & Technology*. 35(21):4189–4197. https://doi.org/10.1021/es0015545

Ancelet T, Davy PK. 2015. Multi-elemental analysis of PM_{10} and apportionment of contributing sources. Lower Hutt (NZ): GNS Science. 10 p. Consultancy Report 2015/117LR. Prepared for Waikato Regional Council.

Ancelet T, Davy PK, Trompetter WJ, Markwitz A, Weatherburn DC. 2011a. Carbonaceous aerosols in an urban tunnel. *Atmospheric Environment*. 45(26):4463–4469. https://doi.org/10.1016/j.atmosenv.2011.05.032

Ancelet T, Davy PK, Trompetter WJ, Markwitz A, Weatherburn DC. 2011b. Characterisation of particulate matter emissions from a modern wood burner under varying burner conditions. *Air Quality and Climate Change*. 45(2):21–27.

Ancelet T, Davy PK, Mitchell T, Trompetter WJ, Markwitz A, Weatherburn DC. 2012. Identification of particulate matter sources on an hourly time-scale in a wood burning community. *Environmental Science & Technology*. 46(9):4767–4774. https://doi.org/10.1021/es203937y

Ancelet T, Davy PK, Trompetter WJ. 2013a. Source apportionment of PM_{10} and $PM_{2.5}$ in Nelson Airshed A. Lower Hutt (NZ): GNS Science. 95 p. Consultancy Report 2013/146. Prepared for Nelson City Council.

Ancelet T, Davy PK, Trompetter WJ, Markwitz A, Weatherburn DC. 2013b. Carbonaceous aerosols in a wood burning community in rural New Zealand. *Atmospheric Pollution Research*. 4(3):245–249. https://doi.org/10.5094/APR.2013.026

Ancelet T, Davy PK, Trompetter WJ. 2014a. Hourly concentrations of arsenic associated with particulate matter. In: Litter MI, Nicolli HB, Meichtry M, Quici N, Bundschuh J, Bhattacharya P, Naidu R, editors. *One century of the discovery of arsenicosis in Latin America (1914–2014), As 2014: proceedings of the 5th International Congress on Arsenic in the Environment*; 2014 May 11–16; Buenos Aires, Argentina. Boca Raton (FL): CRC Press. p. 75–76.

Ancelet T, Davy PK, Trompetter WJ, Markwitz A. 2014b. Sources of particulate matter pollution in a small New Zealand city. *Atmospheric Pollution Research*. 5(4):572–580. https://doi.org/10.5094/APR.2014.066

Ancelet T, Davy PK, Trompetter WJ, Markwitz A, Weatherburn DC. 2014c. Sources and transport of particulate matter on an hourly time-scale during the winter in a New Zealand urban valley. *Urban Climate*. 10:644–655. https://doi.org/10.1016/j.uclim.2014.06.003

Ancelet T, Davy PK, Trompetter WJ. 2015. Particulate matter sources and long-term trends in a small New Zealand city. *Atmospheric Pollution Research*. 6(6):1105–1112. https://doi.org/10.1016/j.apr.2015.06.008

Anlauf K, Li S-M, Leaitch R, Brook J, Hayden K, Toom-Sauntry D, Wiebe A. 2006. Ionic composition and size characteristics of particles in the Lower Fraser Valley: Pacific 2001 field study. *Atmospheric Environment*. 40(15):2662–2675. https://doi.org/10.1016/j.atmosenv.2005.12.027

Ashbaugh LL, Malm WC, Sadeh WZ. 1985. A residence time probability analysis of sulfur concentrations at grand Canyon National Park. *Atmospheric Environment (1967)*. 19(8):1263–1270. https://doi.org/10.1016/0004-6981(85)90256-2

Banari A, Hertel D, Schlink U, Hampel U, Lecrivain G. 2023. Simulation of particle resuspension by wind in an urban system. *Environmental Fluid Mechanics*. 23(1):41–63. https://doi.org/10.1007/s10652-022-09905-x

Begum BA, Hopke PK, Zhao W. 2005. Source identification of fine particles in Washington, DC, by expanded factor analysis modeling. *Environmental Science & Technology*. 39(4):1129–1137. https://doi.org/10.1021/es049804v

Bennett J, Davy P, Trompetter B, Wang Y, Pierse N, Boulic M, Phipps R, Howden-Chapman P. 2019. Sources of indoor air pollution at a New Zealand urban primary school; a case study. *Atmospheric Pollution Research*. 10(2):435–444. https://doi.org/10.1016/j.apr.2018.09.006

Bond TC, Streets DG, Yarber KF, Nelson SM, Woo J-H, Klimont Z. 2004. A technology-based global inventory of black and organic carbon emissions from combustion. *Journal of Geophysical Research: Atmospheres*. 109(D14):D14203. https://doi.org/10.1029/2003JD003697

Bond TC, Doherty SJ, Fahey DW, Forster PM, Berntsen T, DeAngelo BJ, Flanner MG, Ghan S, Kärcher B, Koch D, et al. 2013. Bounding the role of black carbon in the climate system: a scientific assessment. *Journal of Geophysical Research: Atmospheres*. 118(11):5380–5552. https://doi.org/10.1002/jgrd.50171

Brimblecombe P. 1986. Air: composition & chemistry. Cambridge (GB): Cambridge University Press. 224 p.

Brown SG, Hafner HR. 2005. Multivariate receptor modelling workbook. Research Triangle Park (NC): United States Environmental Protection Agency.

Brown SG, Eberly S, Paatero P, Norris GA. 2015. Methods for estimating uncertainty in PMF solutions: examples with ambient air and water quality data and guidance on reporting PMF results. *Science of the Total Environment*. 518–519:626–635. https://doi.org/10.1016/j.scitotenv.2015.01.022

Cahill TA, Eldred RA, Motallebi N, Malm WC. 1989. Indirect measurement of hydrocarbon aerosols across the United States by nonsulfate hydrogen-remaining gravimetric mass correlations. *Aerosol Science and Technology*. 10(2):421–429. https://doi.org/10.1080/02786828908959281

Carslaw DC. 2012. The openair manual: open-source tools for analysing air pollution data – manual for version 0.7-0. London (GB): King's College London.

Carslaw DC, Ropkins K. 2012. openair – an R package for air quality data analysis. *Environmental Modelling & Software*. 27–28:52–61. https://doi.org/10.1016/j.envsoft.2011.09.008

Chueinta W, Hopke PK, Paatero P. 2000. Investigation of sources of atmospheric aerosol at urban and suburban residential areas in Thailand by positive matrix factorization. *Atmospheric Environment*. 34(20):3319–3329. https://doi.org/10.1016/S1352-2310(99)00433-1

Cohen D. 1999. Accelerator based ion beam techniques for trace element aerosol analysis. In: Landsberger S, Creatchman M, editors. *Elemental analysis of airborne particles*. Amsterdam (NL): Gordon and Breach Science Publishers. p. 139–196. (Advances in environmental, industrial, and process control technologies; 1).

Cohen DD, Bailey GM, Kondepudi R. 1996. Elemental analysis by PIXE and other IBA techniques and their application to source fingerprinting of atmospheric fine particle pollution. *Nuclear Instruments and Methods in Physics Research Section B: Beam Interactions with Materials and Atoms*. 109–110:218–226. https://doi.org/10.1016/0168-583X(95)00912-4

Cohen D, Taha G, Stelcer E, Garton D, Box G. 2000. The measurement and sources of fine particle elemental carbon at several key sites in NSW over the past eight years. In: *Proceedings of the 15th International Clean Air and Environment Conference*; 2000 Nov 26–30; Sydney, Australia. Mooroolbark (AU): Clean Air Society of Australia and New Zealand. p. 485–490.

Davy PK, Trompetter WJ. 2017a. Apportionment of PM_{10} sources in the Tokoroa airshed, Waikato region. Lower Hutt (NZ): GNS Science. 55 p. Consultancy Report 2017/75. Prepared for Waikato Regional Council.

Davy PK, Trompetter WJ. 2017b. Source apportionment of $PM_{2.5}$ and PM_{10} sources in the Richmond airshed, Tasman District. Lower Hutt (NZ): GNS Science. 69 p. Consultancy Report 2017/86. Prepared for Tasman District Council.

Davy PK, Trompetter WJ. 2018. Heavy metals, black carbon and natural sources of particulate matter in New Zealand. Lower Hutt (NZ): GNS Science. 81 p. Consultancy Report 2017/238. Prepared for Ministry for the Environment.

Davy PK, Trompetter WJ. 2020. Composition, sources and long-term trends for Auckland air particulate matter: summary report. Lower Hutt (NZ): GNS Science. 32 p. + appendices. Consultancy Report 2019/151. Prepared for Auckland Council.

Davy PK, Trompetter WJ. 2023. Motueka: composition and sources of $PM_{2.5}$. Lower Hutt (NZ): GNS Science. 46 p. Consultancy Report 2023/77. Prepared for Tasman District Council.

Davy PK, Trompetter WJ. 2024. Air particulate matter composition and sources of air pollution in Hastings. Lower Hutt (NZ): GNS Science. 61 p. Consultancy Report 2023/76. Prepared for Hawke's Bay Regional Council.

Davy PK, Markwitz A, Weatherburn DC. 2007. Composition, size and morphological comparison of wood smoke particles from source emissions and in urban air by SEM-EDS. In: *14th IUAPPA World Congress, 2007: clean air partnerships, coming together for clean air: conference proceedings: incorporating the 18th CASANZ Conference*; 2007 Sep 9–13; Brisbane, Australia. Mooroolbark (AU): Clean Air Society of Australia and New Zealand. Paper CC50.

Davy PK, Ancelet T, Trompetter WJ, Markwitz A, Weatherburn DC. 2012. Composition and source contributions of air particulate matter pollution in a New Zealand suburban town. *Atmospheric Pollution Research*. 3(1):143–147. https://doi.org/10.5094/APR.2012.014

Davy PK, Ancelet T, Trompetter WJ, Markwitz A. 2014. Arsenic and air pollution in New Zealand. In: Litter MI, Nicolli HB, Meichtry M, Quici N, Bundschuh J, Bhattacharya P, Naidu R, editors. *One century of the discovery of arsenicosis in Latin America (1914–2014), As 2014: proceedings of the 5th International Congress on Arsenic in the Environment*; 2014 May 11–16; Buenos Aires, Argentina. Boca Raton (FL): CRC Press. p. 394–395.

Davy PK, Ancelet T, Trompetter WJ. 2016. Source apportionment of $PM_{2.5}$ and $PM_{10–2.5}$ samples from St Albans, Christchurch. Lower Hutt (NZ): GNS Science. 61 p. Consultancy Report 2016/72. Prepared for Environment Canterbury.

Davy PK, Ancelet T, Trompetter WJ, Markwitz A. 2017. Source apportionment and trend analysis of air particulate matter in the Auckland region. Lower Hutt (NZ): GNS Science. 245 p. Consultancy Report 2014/194. Prepared for Auckland Council.

Davy PK, Trompetter WJ, Revell LE, Hardacre C. 2024. Evaluation of New Zealand's background particulate matter sources. Lower Hutt (NZ): GNS Science. 98 p. Consultancy Report 2024/53. Prepared for the Ministry for the Environment.

Dockery DW, Luttmann-Gibson H, Rich DQ, Link MS, Mittleman MA, Gold DR, Koutrakis P, Schwartz JD, Verrier RL. 2005. Association of air pollution with increased incidence of ventricular tachyarrhythmias recorded by implanted cardioverter defibrillators. *Environmental Health Perspectives*. 113(6):670–674. https://doi.org/10.1289/ehp.7767

Eberly SI. 2005. EPA PMF 1.1 User's Guide. Washington (DC): United States Environmental Protection Agency. EPA/600/R-06/166.

Fine PM, Cass GR, Simoneit BRT. 2001. Chemical characterization of fine particle emissions from fireplace combustion of woods grown in the northeastern United States. *Environmental Science & Technology*. 35(13):2665–2675. https://doi.org/10.1021/es001466k

Fitzgerald JW. 1991. Marine aerosols: a review. *Atmospheric Environment Part A General Topics*. 25(3–4):533–545. https://doi.org/10.1016/0960-1686(91)90050-H

Gard EE, Kleeman MJ, Gross DS, Hughes LS, Allen JO, Morrical BD, Fergenson DP, Dienes T, Gälli ME, Johnson RJ, et al. 1998. Direct observation of heterogeneous chemistry in the atmosphere. *Science*. 279(5354):1184–1187. https://doi.org/10.1126/science.279.5354.1184

Geng F, Hua J, Mu Z, Peng L, Xu X, Chen R, Kan H. 2013. Differentiating the associations of black carbon and fine particle with daily mortality in a Chinese city. *Environmental Research*. 120:27–32. https://doi.org/10.1016/j.envres.2012.08.007

George IJ, Abbatt JPD. 2010. Heterogeneous oxidation of atmospheric aerosol particles by gas-phase radicals. *Nature Chemistry*. 2(9):713–722. https://doi.org/10.1038/nchem.806

Grange SK, Salmond JA, Trompetter WJ, Davy PK, Ancelet T. 2013. Effect of atmospheric stability on the impact of domestic wood combustion to air quality of a small urban township in winter. *Atmospheric Environment*. 70:28–38. https://doi.org/10.1016/j.atmosenv.2012.12.047

Hays MD, Cho S-H, Baldauf R, Schauer JJ, Shafer M. 2011. Particle size distributions of metal and non-metal elements in an urban near-highway environment. *Atmospheric Environment*. 45(4):925–934. https://doi.org/10.1016/j.atmosenv.2010.11.010

Hopke PK. 1999. An introduction to source receptor modeling. In: Landsberger S, Creatchman M, editors. *Elemental analysis of airborne particles*. Amsterdam (NL): Gordon and Breach Science Publishers. p. 273–315. (Advances in environmental, industrial, and process control technologies; 1).

Hopke PK. 2003. Recent developments in receptor modeling. *Journal of Chemometrics*. 17(5):255–265. https://doi.org/10.1002/cem.796

Hopke PK, Xie Y, Paatero P. 1999. Mixed multiway analysis of airborne particle composition data. *Journal of Chemometrics*. 13(3–4):343–352. https://doi.org/10.1002/(SICI)1099-128X(199905/08)13:3/4<343::AID-CEM550>3.0.CO;2-P

Horvath H. 1993. Atmospheric light absorption: a review. *Atmospheric Environment Part A: General Topics*. 27(3):293–317. https://doi.org/10.1016/0960-1686(93)90104-7

Horvath H. 1997. Experimental calibration for aerosol light absorption measurements using the integrating plate method – summary of the data. *Journal of Aerosol Science*. 28(7):1149–1161. https://doi.org/10.1016/S0021-8502(97)00007-4

Huang X-F, Yu JZ, He L-Y, Hu M. 2006. Size distribution characteristics of elemental carbon emitted from Chinese vehicles: results of a tunnel study and atmospheric implications. *Environmental Science & Technology*. 40(17):5355–5360. https://doi.org/10.1021/es0607281

Hung NTQ, Lee S-B, Hang NT, Kongpran J, Kim Oanh NT, Shim S-G, Bae G-N. 2014. Characterization of black carbon at roadside sites and along vehicle roadways in the Bangkok metropolitan region. *Atmospheric Environment*. 92:231–239. https://doi.org/10.1016/j.atmosenv.2014.04.011

Jacobson MZ. 2001. Strong radiative heating due to the mixing state of black carbon in atmospheric aerosols. *Nature*. 409(6821):695–697. https://doi.org/10.1038/35055518

Jeong C-H, Hopke PK, Kim E, Lee D-W. 2004. The comparison between thermal-optical transmittance elemental carbon and Aethalometer black carbon measured at multiple monitoring sites. *Atmospheric Environment*. 38(31):5193–5204. https://doi.org/10.1016/j.atmosenv.2004.02.065

Kara M, Hopke P, Dumanoglu Y, Altiok H, Elbir T, Odabasi M, Bayram A. 2015. Characterization of PM using multiple site data in a heavily industrialized region of Turkey. *Aerosol and Air Quality Research*. 15(1):11–27. https://doi.org/10.4209/aaqr.2014.02.0039

Ke L, Ding X, Tanner RL, Schauer JJ, Zheng M. 2007. Source contributions to carbonaceous aerosols in the Tennessee Valley Region. *Atmospheric Environment*. 41(39):8898–8923. https://doi.org/10.1016/j.atmosenv.2007.08.024

Khalil MAK, Rasmussen RA. 2003. Tracers of wood smoke. *Atmospheric Environment*. 37(9):1211–1222. https://doi.org/10.1016/S1352-2310(02)01014-2

Kim E, Hopke PK, Edgerton ES. 2003. Source identification of Atlanta aerosol by positive matrix factorization. *Journal of the Air & Waste Management Association*. 53(6):731–739. https://doi.org/10.1080/10473289.2003.10466209

Kim E, Hopke PK, Larson TV, Maykut NN, Lewtas J. 2004. Factor analysis of Seattle fine particles. *Aerosol Science and Technology*. 38(7):724–738. https://doi.org/10.1080/02786820490490119

Kuschel G, Metcalfe J, Sridhar S, Davy P, Hastings K, Mason K, Denne T, Berentson-Shaw J, Bell S, Hales S, et al. 2022. Health and air pollution in New Zealand 2016 (HAPINZ 3.0): volume 2 – detailed methodology. Auckland (NZ): Emission Impossible Ltd. 218 p. Prepared for the Ministry for the Environment, the Ministry of Health, Te Manatū Waka Ministry of Transport, Waka Kotahi NZ Transport Agency.

Lack DA, Corbett JJ, Onasch T, Lerner B, Massoli P, Quinn PK, Bates TS, Covert DS, Coffman D, Sierau B, et al. 2009. Particulate emissions from commercial shipping: chemical, physical, and optical properties. *Journal of Geophysical Research: Atmospheres*. 114(D7):D00F04. https://doi.org/10.1029/2008jd011300

Lee E, Chan CK, Paatero P. 1999. Application of positive matrix factorization in source apportionment of particulate pollutants in Hong Kong. *Atmospheric Environment*. 33(19):3201–3212. https://doi.org/10.1016/S1352-2310(99)00113-2

Lee JH, Yoshida Y, Turpin BJ, Hopke PK, Poirot RL, Lioy PJ, Oxley JC. 2002. Identification of sources contributing to Mid-Atlantic regional aerosol. *Journal of the Air & Waste Management Association*. 52(10):1186–1205. https://doi.org/10.1080/10473289.2002.10470850

Lide DR. 1992. CRC handbook of chemistry and physics, 1992–1993. 73rd ed. Boca Raton (FL): CRC Press. 1 volume.

Lopez-Reyes A, Orozco-Rivera G, Acuna-Askar K, Villarreal-Chiu JF, Alfaro-Barbosa JM. 2016. Characterization of atmospheric black carbon in particulate matter over the Monterrey metropolitan area, Mexico, using scanning electron microscopy. *Air Quality, Atmosphere & Health*. 9(3):223–229. https://doi.org/10.1007/s11869-015-0328-5

Maenhaut W, Malmqvist KG. 2001. Particle-induced X-ray emission analysis. In: van Grieken R, Markowicz A, editors. *Handbook of X-ray spectrometry*. 2nd ed. New York (NY): Marcel Dekker. p. 719–810.

Malm WC, Sisler JF, Huffman D, Eldred RA, Cahill TA. 1994. Spatial and seasonal trends in particle concentration and optical extinction in the United States. *Journal of Geophysical Research: Atmospheres*. 99(D1):1347–1370. https://doi.org/10.1029/93jd02916

Maxwell JA, Campbell JL, Teesdale WJ. 1989. The Guelph PIXE software package. *Nuclear Instruments and Methods in Physics Research Section B: Beam Interactions with Materials and Atoms*. 43(2):218–230. https://doi.org/10.1016/0168-583X(89)90042-6

Maxwell JA, Teesdale WJ, Campbell JL. 1995. The Guelph PIXE software package II. *Nuclear Instruments and Methods in Physics Research Section B: Beam Interactions with Materials and Atoms*. 95(3):407–421. https://doi.org/10.1016/0168-583X(94)00540-0

Ministry for the Environment. 1997. Environmental performance indicators: proposals for air, freshwater and land. Wellington (NZ): Ministry for the Environment.

Ministry for the Environment. 2002. Ambient Air Quality Guidelines: 2002 update. Wellington (NZ): Ministry for the Environment. 58 p.

Ministry for the Environment. 2011. 2011 users' guide to the revised National Environmental Standards for Air Quality: updated 2014. Wellington (NZ): Ministry for the Environment. 139 p.

Mitchell T, Davy PK, Kim N, Ancelet T, Trompetter WJ. 2013. Arsenic concentrations in a suburban New Zealand wood burning community. In: *21st International Clean Air & Environment Conference: conference proceedings*; 2013 Sep 7–11; Sydney, Australia. Mooroolbark (AU): Clean Air Society of Australia & New Zealand. Paper 101.

Norris G, Duvall R, Brown S, Bai S. 2014. EPA Positive Matrix Factorization (PMF) 5.0 fundamentals and user guide. Washington (DC): US Environmental Protection Agency. 124 p. EPA/600/R-14/108.

O'Dowd CD, Lowe JA, Clegg N, Smith MH, Clegg SL. 2000. Modeling heterogeneous sulphate production in maritime stratiform clouds. *Journal of Geophysical Research: Atmospheres*. 105(D6):7143–7160. https://doi.org/10.1029/1999JD900915

Paatero P. 1997. Least squares formulation of robust non-negative factor analysis. *Chemometrics and Intelligent Laboratory Systems*. 37(1):23–35. https://doi.org/10.1016/S0169-7439(96)00044-5

Paatero P. 2000. PMF User's Guide. Helsinki (FI): University of Helsinki. 2 parts.

Paatero P, Hopke PK. 2002. Utilizing wind direction and wind speed as independent variables in multilinear receptor modeling studies. *Chemometrics and Intelligent Laboratory Systems*. 60(1):25–41. https://doi.org/10.1016/S0169-7439(01)00183-6

Paatero P, Hopke PK. 2003. Discarding or downweighting high-noise variables in factor analytic models. *Analytica Chimica Acta*. 490(1):277–289. https://doi.org/10.1016/S0003-2670(02)01643-4

Paatero P, Hopke PK, Song X-H, Ramadan Z. 2002. Understanding and controlling rotations in factor analytic models. *Chemometrics and Intelligent Laboratory Systems*. 60(1):253–264. https://doi.org/10.1016/S0169-7439(01)00200-3

Paatero P, Hopke PK, Begum BA, Biswas SK. 2005. A graphical diagnostic method for assessing the rotation in factor analytical models of atmospheric pollution. *Atmospheric Environment*. 39(1):193–201. https://doi.org/10.1016/j.atmosenv.2004.08.018

Paatero P, Eberly S, Brown SG, Norris GA. 2014. Methods for estimating uncertainty in factor analytic solutions. *Atmospheric Measurement Techniques*. 7(3):781–797. https://doi.org/10.5194/amt-7-781-2014

Patel H, Talbot N, Salmond J, Dirks K, Xie S, Davy P. 2020. Implications for air quality management of changes in air quality during lockdown in Auckland (New Zealand) in response to the 2020 SARS-CoV-2 epidemic. *Science of the Total Environment*. 746:141129. https://doi.org/10.1016/j.scitotenv.2020.141129

Pósfai M, Simonics R, Li J, Hobbs PV, Buseck PR. 2003. Individual aerosol particles from biomass burning in southern Africa: 1. Compositions and size distributions of carbonaceous particles. *Journal of Geophysical Research: Atmospheres*. 108(D13):8483. https://doi.org/10.1029/2002JD002291

Pósfai M, Gelencsér A, Simonics R, Arató K, Li J, Hobbs PV, Buseck PR. 2004. Atmospheric tar balls: particles from biomass and biofuel burning. *Journal of Geophysical Research: Atmospheres*. 109(D6):D06213. https://doi.org/10.1029/2003JD004169

R Core Team. 2015. R: a language and environment for statistical computing. Vienna (AT): R Foundation for Statistical Computing.

Ramadan Z, Eickhout B, Song X-H, Buydens LMC, Hopke PK. 2003. Comparison of Positive Matrix Factorization and Multilinear Engine for the source apportionment of particulate pollutants. *Chemometrics and Intelligent Laboratory Systems*. 66(1):15–28. https://doi.org/10.1016/S0169-7439(02)00160-0

Salako GO, Hopke PK, Cohen DD, Begum BA, Biswas SK, Pandit GG, Lodoysamba S, Wimolwattanapun W, Bunprapob S, Chung Y-S, et al. 2012. Exploring the variation between EC and BC in a variety of locations. *Aerosol and Air Quality Research*. 12(1):1–7. https://doi.org/10.4209/aaqr.2011.09.0150

Schneider J, Kirchner U, Borrmann S, Vogt R, Scheer V. 2008. In situ measurements of particle number concentration, chemically resolved size distributions and black carbon content of traffic-related emissions on German motorways, rural roads and in city traffic. *Atmospheric Environment*. 42(18):4257–4268. https://doi.org/10.1016/j.atmosenv.2008.01.014

Scott A. 2014. Timaru source apportionment study. Christchurch (NZ): Environment Canterbury Regional Council. 30 p. Technical Report 12/100.

Seinfeld JH, Pandis SN. 2006. Atmospheric chemistry and physics: from air pollution to climate change. 2nd ed. Hoboken (NJ): John Wiley. 1203 p.

Song X-H, Polissar AV, Hopke PK. 2001. Sources of fine particle composition in the northeastern US. *Atmospheric Environment*. 35(31):5277–5286. https://doi.org/10.1016/S1352-2310(01)00338-7

Thorpe A, Harrison RM. 2008. Sources and properties of non-exhaust particulate matter from road traffic: a review. *Science of the Total Environment*. 400(1–3):270–282. https://doi.org/10.1016/j.scitotenv.2008.06.007

Trompetter WJ. 2004. Ion Beam Analysis results of air particulate filters from the Wellington Regional Council. Lower Hutt (NZ): Institute of Geological & Nuclear Sciences. 17 p. Client Report 2004/24. Prepared for Wellington Regional Council.

Trompetter WJ, Markwitz A, Davy P. 2005. Air particulate research capability at the New Zealand Ion Beam Analysis Facility using PIXE and IBA techniques. *International Journal of PIXE*. 15(03n04):249–255. https://www.worldscientific.com/doi/abs/10.1142/S0129083505000581

Trompetter WJ, Davy PK, Markwitz A. 2010. Influence of environmental conditions on carbonaceous particle concentrations within New Zealand. *Journal of Aerosol Science*. 41(1):134–142. https://doi.org/10.1016/j.jaerosci.2009.11.003

Trompetter WJ, Grange SK, Davy PK, Ancelet T. 2013. Vertical and temporal variations of black carbon in New Zealand urban areas during winter. *Atmospheric Environment*. 75:179–187. https://doi.org/10.1016/j.atmosenv.2013.04.036

[WHO] World Health Organization. 2021. WHO global air quality guidelines: particulate matter ($PM_{2.5}$ and PM_{10}), ozone, nitrogen dioxide, sulfur dioxide and carbon monoxide. Bonn (DE): World Health Organization. 273 p.

Wilton E, Davy P, Smith J. 2007. Source identification and apportionment of PM_{10} and $PM_{2.5}$ in Hastings and Auckland. Christchurch (NZ): National Institute of Water & Atmospheric Research. 87 p. Client Report CHC2007-137. Prepared for the Foundation for Science, Research and Technology.

Zanobetti A, Schwartz J. 2006. Air pollution and emergency admissions in Boston, MA. *Journal of Epidemiology and Community Health*. 60(10):890–895. http://doi.org/10.1136/jech.2005.039834

This page left intentionally blank.

APPENDICES

This page left intentionally blank.

APPENDIX 1 ANALYSIS TECHNIQUES

A1.1 Ion Beam Analysis

Ion beam analysis (IBA) was used to measure the elemental concentrations of particulate matter on the size-resolved filter samples from the Hastings monitoring site. IBA is based on the measurement of characteristic X-rays and γ-rays of an element produced by ion-atom interactions using high-energy protons in the 2–5 million electron volt (MeV) range. IBA is a mature and well-developed science, with many research groups around the world using IBA in a variety of routine analytical applications, including the analysis of atmospheric aerosols (Maenhaut and Malmqvist 2001; Trompetter et al. 2005). IBA techniques do not require sample preparation and are fast, non-destructive and sensitive (Cohen 1999; Maenhaut and Malmqvist 2001; Trompetter et al. 2005).

IBA measurements for this study were carried out at the New Zealand IBA facility operated by GNS Science. Figure A1.1 shows the particulate-matter analysis chamber with its associated X-ray, γ-ray and particle detectors for Particle-Induced X-ray Emission (PIXE), Particle-Induced Gamma-ray Emission (PIGE), Proton Elastic Scattering Analysis (PESA) and Rutherford Back Scattering (RBS) measurements.

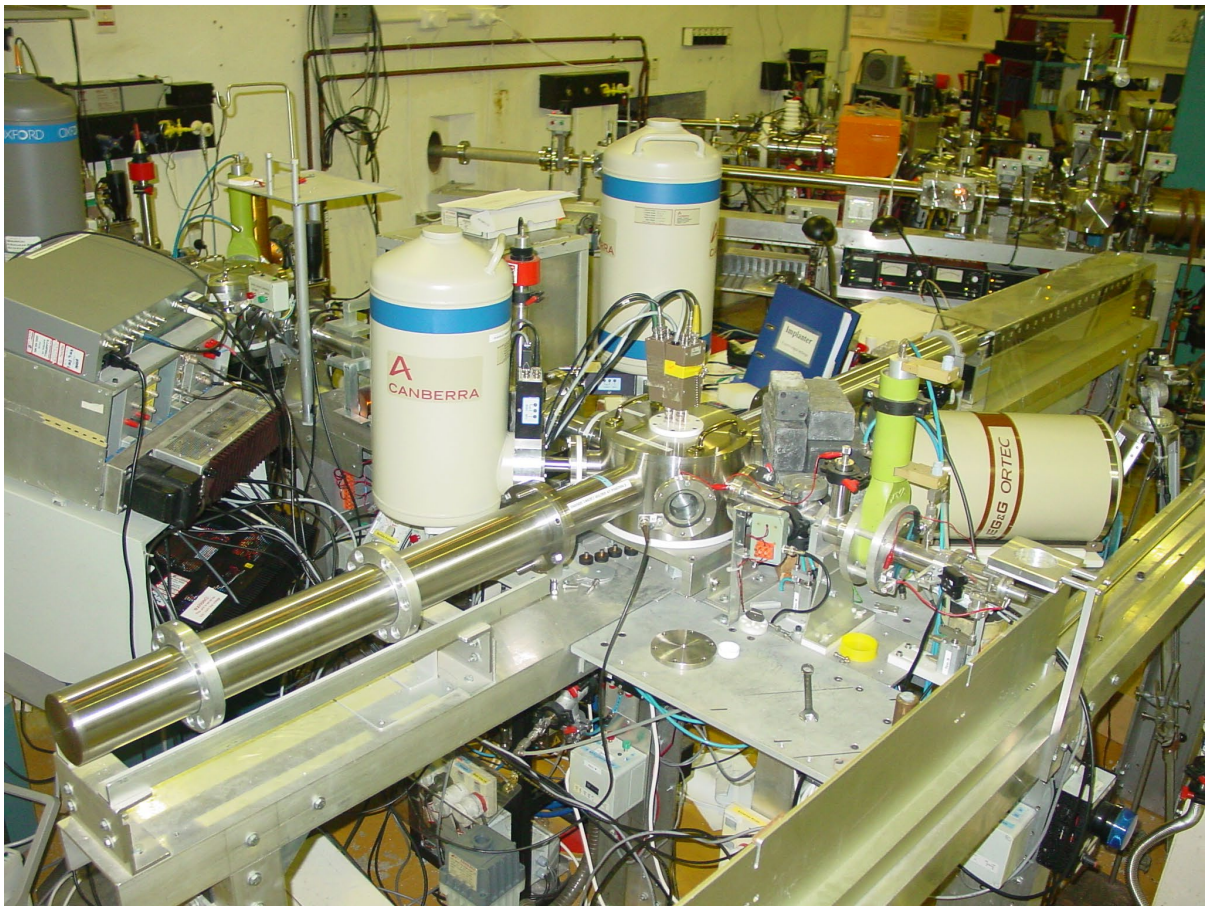

Figure A1.1 Particulate-matter analysis chamber with its associated detectors.

The following sections provide a generalised overview of the IBA techniques used for elemental analysis and the analytical set-up at GNS Science (Cohen 1999; Cohen et al. 1996; Trompetter 2004; Trompetter et al. 2005). Figure A1.2 presents a schematic diagram of the typical experimental set-up for IBA of air-particulate filters at GNS Science.

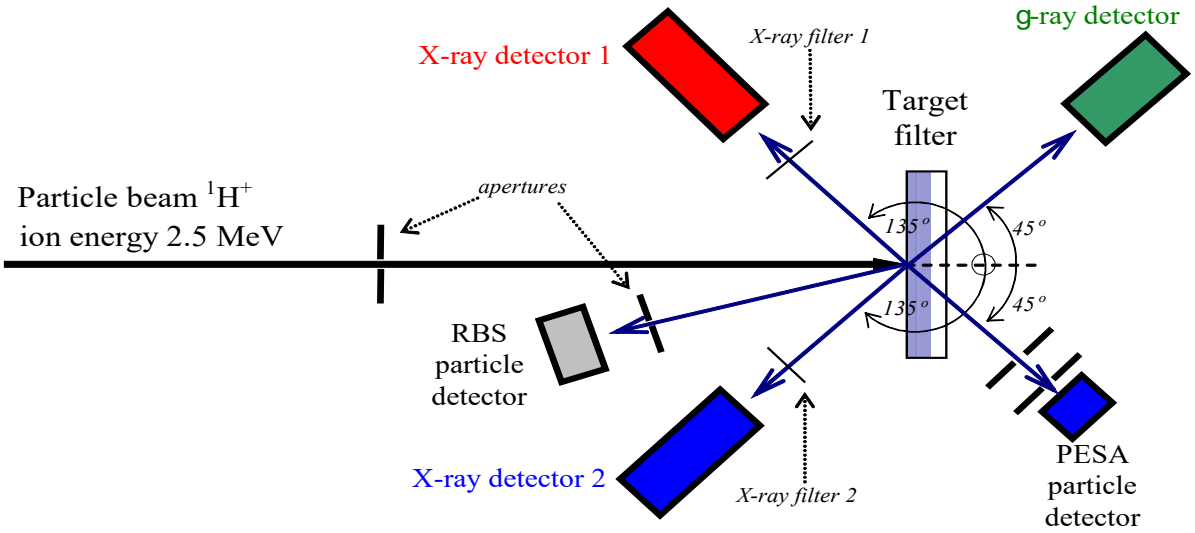

Figure A1.2 Schematic of the typical ion beam analysis experimental set-up at GNS Science.

A1.2 Particle-Induced X-Ray Emission

Particle-induced X-ray emission (PIXE) is used to determine elemental concentrations heavier than neon by exposing the filter samples to a proton beam accelerated to 2.5 MeV by the GNS Science 3 MeV van-de-Graaff accelerator. When high-energy protons interact with atoms in the sample, characteristic X-rays (from each element) are emitted by ion-electron processes. These X-rays are recorded in an energy spectrum. While all elements heavier than boron emit K X-rays, their production becomes too few to satisfactorily measure elements heavier than strontium. Elements heavier than strontium are detected via their lower-energy L X-rays. The X-rays are detected using a Si(Li) detector, and the pulses from the detector are amplified and recorded in a pulse height analyser. In practise, sensitivities are further improved for the lighter elements by using two X-ray detectors, one for light element X-rays and the other for heavier element X-rays, each with different filtering and collimation. Figure A1.3 shows an example of a PIXE spectrum for airborne particles collected on a filter and analysed at the GNS Science IBA facility.

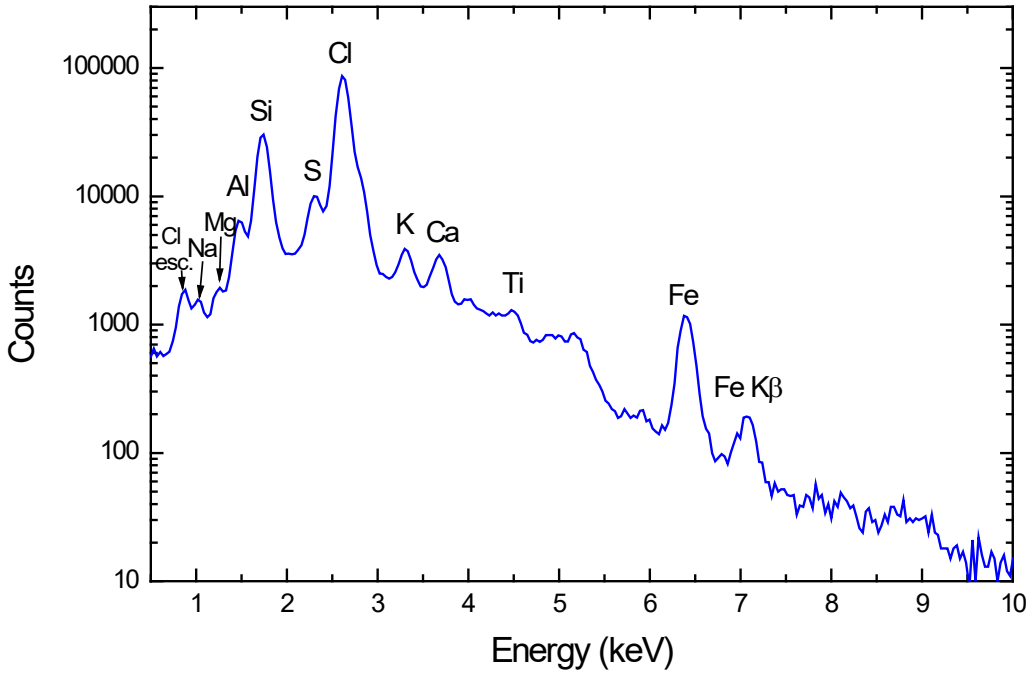

Figure A1.3 Typical spectrum for an aerosol sample analysed by particle-induced X-ray emission (PIXE).

As the PIXE spectrum consists of many peaks from different elements (and a Bremsstrahlung background), some of them overlapping, the spectrum is analysed with quantitative X-ray analysis software. In the case of this study, GUPIX software was used to perform the de-convolution with high accuracy (Maxwell et al. 1989, 1995). The number of pulses (counts) in each peak for a given element is used by the GUPIX software to calculate the concentration of that element. The background and neighbouring elements determine the statistical error and limit of detection. Note that GUPIX provides a specific statistical error and limit of detection for each element in any filter, which is essential for source apportionment studies.

Typically, 20–25 elements from Mg to Pb are routinely determined above their respective limits of detection. Sodium (and fluorine) was determined using both PIXE and PIGE (see next section). Specific experimental details, where appropriate, are given in the results and analysis section.

A1.3 Particle-Induced Gamma-Ray Emission

Particle-induced Gamma-Ray emission (PIGE) refers to γ-rays produced when an incident beam of protons interacts with the nuclei of an element in the sample (filter). During the de-excitation process, nuclei emit γ-ray photons of characteristic energies specific to each element. Typical elements measured with γ-rays are:

Element	Nuclear Reaction	Gamma Ray Energy (keV)
Sodium	$^{23}Na(p,\alpha\gamma)^{20}Ne$	440, 1634
Fluorine	$^{19}F(p,\alpha\gamma)^{16}O$	197, 6129

Gamma rays are higher in energy than X-rays and are detected with a germanium detector. Measurements of a light element such as sodium can be measured more accurately using PIGE because the γ-rays are not attenuated to the same extent in the filter matrix or detector material, a problem in the measurement of low-energy X-rays of sodium. Figure A1.4 shows a typical PIGE spectrum.

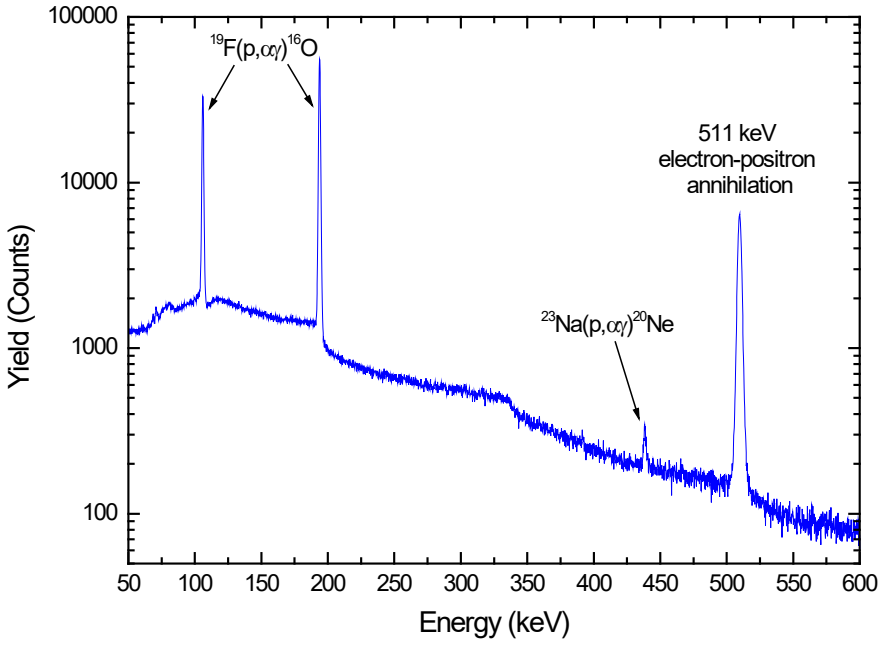

Figure A1.4 Typical particle-induced gamma-ray emission (PIGE) spectrum for an aerosol sample.

A1.4 Ion Beam Analysis Data Reporting

Most filters used to collect particulate matter samples for IBA analysis are sufficiently thin that the ion beam penetrates the entire depth, producing a quantitative analysis of elements present. Because of the thin nature of the air-particulate-matter filters, the concentrations reported from the analyses are therefore in aerial density units (ng cm^{-2}), and the total concentration of each element on the filters is calculated by multiplying with the exposed area of the filter. Typically, the exposed area is approximately 0.16 cm^2 for the sample deposit on the Streaker filters used in this study. For example, to convert from Cl (ng cm^{-2}) into Cl (ng m^{-3}) for Streaker filter samples, the equation is:

$$Cl\ (ng\ m^{-3}) = 0.16\ (cm^2) \times Cl\ (ng\ cm^{-2}) / Vol(m^3)$$

A1.4.1 Limits of Detection and Uncertainty Reporting for Elements

The exact limits of detection and associated analytical uncertainties for the concentration of each element depends on a number of factors such as:

- method of detection
- filter composition
- sample composition
- detector resolution, and
- spectral interference from other elements.

Also, where an individual elemental concentration is reported as zero (0), this means that the measurement value (as derived from the spectral de-convolution) was zero but does not necessarily mean that the element was not present; instead, it was below the method limit of detection and indeterminate. Where this is the case, the corresponding uncertainty value (±) can then be regarded as 5/6 limit of detection (Kara et al. 2015).

For IBA, to determine the concentration of each element, the background is subtracted and peak areas fitted and calculated. The background occurs through energy loss, scattering any interactions of the ion beam as it passes through the filter material, or from γ-rays produced in the target and scattered in the detector system (Cohen 1999). The peaks of elements in spectra that have interferences or backgrounds from other elements present in the air-particulate matter, or filter matrix itself, will have higher limits of detection. The IBA was performed using a 3 MeV accelerator proton beam with standards (SrF2, NaCl, Cr, Ni, SiO, KCl, Al) run before and after each analytical cycle. Spectral X-ray peak de-convolution was performed using GUPIX software (Maxwell et al. 1989, 1995). The number of pulses (counts) in each peak for a given element is used by the GUPIX software to calculate the concentration of that element. The background and neighbouring elements determine the statistical error and limit of detection. Note that GUPIX provides a specific statistical error (uncertainty) and limit of detection for each element in each particulate-matter sample. The statistical uncertainty is calculated from the X-ray peak-fitting process (called the fit error) and is related to the square root of the peak area. The limit of detection for an element in each sample spectra is defined as three times the error (3σ) obtained for the background and overlap (but not the element's own area) in a one full-width-half-maximum region centred about the principal X-ray peak of the element. The summary statistics provided for elemental concentrations in each dataset are therefore averages of the individual uncertainty and limit of detection values.

Choice of filter material is an important consideration with respect to elements of interest, as is avoiding sources of contamination. The GNS Science IBA laboratory routinely runs filter blanks to correct for filter-derived analytical artefacts as part of its quality assurance and control procedures. Figure A1.5 shows the limits of detection typically achieved by PIXE for each element at the GNS Science IBA facility. All IBA elemental concentrations determined in this work were accompanied by their respective limits of detection. The use of elemental limits of detection is important in receptor-modelling applications.

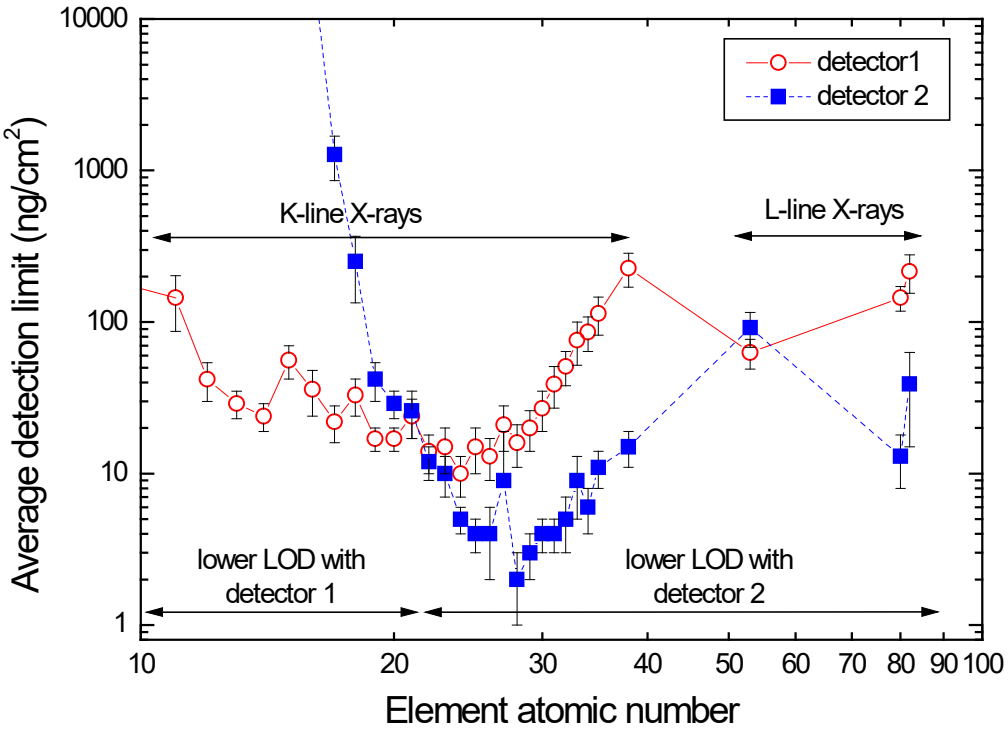

Figure A1.5 Elemental limits of detection for particle-induced X-ray emission (PIXE) routinely achieved at the GNS Science Ion Beam Analysis facility for air filters.

A1.5 Black Carbon Measurements

Black carbon is a combustion-derived atmospheric aerosol that has important implications for human health and the Earth's climate. Exposure to ambient concentrations of black carbon has been associated with significant negative impacts on human health, including increased hospital admissions and mortality due to cardiovascular diseases (Dockery et al. 2005; Zanobetti and Schwartz 2006; Geng et al. 2013). Black carbon also plays a unique role in the Earth's climate system. While most aerosols in the atmosphere scatter incoming solar radiation, resulting in a net cooling effect on the atmosphere, black carbon absorbs significantly more light than it reflects, resulting in a net warming effect. Light-absorbing particles radiate long-wave energy that heats the surrounding air. This results in a positive (warming) forcing (Jacobson 2001). The magnitude of black carbon's warming has been estimated to be the second-highest warming species, trailing only the effects of carbon dioxide (Bond et al. 2013). Research regarding the concentrations and effects of black carbon is ongoing, and, as more research is undertaken, it is likely that these and other effects will be further quantified.

Black carbon particle size ranges have been well characterised over a variety of emission sources, both in New Zealand (Davy et al. 2007; Ancelet et al. 2011a, 2011b; Davy et al. 2012; Salako et al. 2012; Ancelet et al. 2013b; Trompetter et al. 2013) and internationally (Ke et al. 2007; Schneider et al. 2008; Lack et al. 2009; Hays et al. 2011; Lopez-Reyes et al. 2016) and are invariably found to be in the sub-micrometre size range. Black carbon particles can

consist of individual spherules (10–30 nm in diameter) to larger agglomerations (300–500 nm diameter) of individual particles. Black carbon (often called 'soot') is usually formed under conditions in which insufficient oxygen is present for complete oxidation of carbonaceous fuel to CO_2 (fuel-rich) (Bond et al. 2004). The characteristics of the combustion source therefore have an important bearing on particle size and carbonaceous composition, with high-temperature combustion conditions (diesel engines, power stations) producing smaller, graphitic carbon particle entities (Allen et al. 2001; Huang et al. 2006; Ancelet et al. 2011a; Hung et al. 2014), whereas lower-temperature biomass combustion (wood fires for home heating, wild fire, forest fires) produces a mixture of carbon agglomerations and larger particles (500–900 nm) composed of a soot core and coated in organic 'tar' from incomplete combustion (Pósfai et al. 2003, 2004; Davy et al. 2007).

Determination of carbon (soot) on filters was performed by light reflection to provide the black carbon concentration. The absorption and reflection of visible light on particles in the atmosphere or collected on filters is dependent on the particle concentration, density, refractive index and size. For atmospheric particles, black carbon is the most highly absorbing component in the visible light spectrum, with much smaller components coming from soils, sulphates and nitrate (Horvath 1993, 1997). Hence, to the first order, it can be assumed that all of the absorption on atmospheric filters is due to black carbon. The main sources of atmospheric black carbon are anthropogenic combustion sources and include biomass burning, motor vehicles and industrial emissions (Cohen et al. 2000). Cohen and co-workers found that black carbon is typically 10–40% of the fine mass ($PM_{2.5}$) fraction in many urban areas of Australia.

When measuring black carbon by light reflection/transmission, light from a light source is transmitted through a filter onto a photocell. The amount of light absorption is proportional to the amount of black carbon present and provides a value that is a measure of the black carbon on the filter. Conversion of the absorbance value to an atmospheric concentration value of black carbon (*BC*) requires the use of an empirically derived equation (Cohen et al. 2000):

$$BC\ (\mu g\ cm^{-2}) = (100/2(F\varepsilon))\ ln[R_0/R] \qquad \text{Equation A1.1}$$

where:

- ε is the mass absorbent coefficient for *BC* ($m^2\ g^{-1}$) at a given wavelength.
- *F* is a correction factor to account for other absorbing factors such as sulphates, nitrates, shadowing and filter loading. These effects are generally assumed to be negligible, and *F* is set at 1.00.
- R_0 and *R* are the pre- and post-reflection intensity measurements, respectively.

Black carbon was measured at GNS Science using the M43D Digital Smoke Stain Reflectometer. The following equation (from Willy Maenhaut, Institute for Nuclear Sciences, University of Gent, Belgium) was used for obtaining black carbon from reflectance measurements on Nucleopore polycarbonate filters or Pall Life Sciences Teflon filters:

$$BC\ (\mu g\ cm^{-2}) = [1000 \times LOG(R_{blank}/R_{sample}) + 2.39] / 45.8 \qquad \text{Equation A1.2}$$

where:

- R_{blank} is the average reflectance for a series of blank filters; it is close (but not identical) to 100. GNS Science always uses the same blank filter for adjusting to 100.
- R_{sample} is the reflectance for a filter sample (normally lower than 100).

with 2.39 and 45.8 constants derived using a series of 100 Nuclepore polycarbonate filter samples, which served as secondary standards; the black carbon loading (in μg cm^{-2}) for these samples had been determined by Prof. Dr. MO Andreae (Max Planck Institute of Chemistry, Mainz, Germany) relative to standards that were prepared by collecting burning acetylene soot on filters and determining the mass concentration gravimetrically (Trompetter 2004).

A1.6 Positive Matrix Factorisation

PMF is a linear least-squares approach to factor analysis and was designed to overcome the receptor modelling problems associated with techniques such as principal components analysis (PCA) and the *a priori* knowledge required for chemical mass balance approaches (Paatero et al. 2005). With PMF, sources are constrained to have non-negative species concentrations, no sample can have a negative source contribution and error estimates for each observed data point are used as point-by-point weights. This feature is a distinct advantage in that it can accommodate missing and below-detection-limit data that is a common feature of environmental monitoring results (Song et al. 2001). In fact, the signal-to-noise ratio for an individual elemental measurement can have a significant influence on a receptor model and modelling results. For the weakest (closest to detection limit) species, the variance may be entirely from noise (Paatero and Hopke 2002). Paatero and Hopke (2002) strongly suggest down-weighting or discarding noisy variables that are always below their detection limit or species that have a lot of error in their measurements relative to the magnitude of their concentrations (Paatero and Hopke 2003). The distinct advantage of PMF is that mass concentrations can be included in the model and the results are directly interpretable as mass contributions from each factor (source).

A1.7 Positive Matrix Factorisation Model Outline

The mathematical basis for PMF is described in detail by Paatero (Paatero 1997, 2000). Briefly, PMF uses a weighted least-squares fit with the known error estimates of measured elemental concentrations used to derive the weights. In matrix notation, this is indicated as:

$$X = GF + E \qquad \text{Equation A1.3}$$

where:

- X is the known n x m matrix of m measured elemental species in n samples.
- G is an n x p matrix of source contributions to the samples.
- F is a p x m matrix of source compositions (source profiles).
- E is a residual matrix – the difference between measurement X and model Y.

E can be defined as a function of factors G and F:

$$e_{ij} = x_{ij} - y_{ij} = x_{ij} - \sum_{k=1}^{p} g_{ik} f_{kj} \qquad \text{Equation A1.4}$$

where:

- i = 1,……,n elements.
- j = 1,……,m samples.
- k = 1,…...,p sources.

PMF constrains all elements of *G* and *F* to be non-negative, meaning that elements cannot have negative concentrations and samples cannot have negative source contributions as in real space. The task of PMF is to minimise the function *Q* such that:

$$Q(E) = \sum_{i=1}^{n} \sum_{j=1}^{m} (e_{ik} / \sigma_{kj})^2 \qquad \text{Equation A1.5}$$

where σ_{kj} is the error estimate for x_{ij}. Another advantage of PMF is the ability to handle extreme values typical of air-pollutant concentrations, as well as true outliers that would normally skew PCA. In either case, such high values would have significant influence on the solution (commonly referred to as leverage). PMF has been successfully applied to receptor modelling studies in a number of countries around the world (Hopke et al. 1999; Lee et al. 1999; Chueinta et al. 2000; Song et al. 2001; Lee et al. 2002; Kim et al. 2003; Jeong et al. 2004; Kim et al. 2004; Begum et al. 2005), including New Zealand (Ancelet et al. 2012; Davy et al. 2012; Ancelet et al. 2014c; Bennett et al. 2019; Davy and Trompetter 2020; Patel et al. 2020).

A1.7.1 Positive Matrix Factorisation Model Used

Two programs have been written to implement different algorithms for solving the least squares PMF problem; these are PMF2 and EPAPMF, and the latter incorporates the Multilinear Engine (ME-2) (Hopke et al. 1999; Ramadan et al. 2003). In effect, the EPAPMF program provides a more flexible framework than PMF2 for controlling the solutions of the factor analysis, with the ability of imposing explicit external constraints.

This study used EPAPMF 5.0 (version 14.0), which incorporates a graphical user interface (GUI) based on the ME-2 program. Both PMF2 and EPAPMF programs can be operated in a robust mode, meaning that 'outliers' are not allowed to overly influence the fitting of the contributions and profiles (Eberly 2005). The user specifies two input files, one file with the concentrations and one with the uncertainties associated with those concentrations. The methodology for developing an uncertainty matrix associated with the elemental concentrations for this work is discussed in Section A1.4.2.

A1.7.2 Positive Matrix Factorisation Model Inputs

The PMF programs provide the user with a number of choices in model parameters that can influence the final solution. Two parameters, the 'signal-to-noise ratio' and the 'species category' are of particular importance and are described below.

Signal-to-noise ratio (S/N): This is a useful diagnostic statistic estimated from the input data and uncertainty files. Two calculations are performed to determine S/N, where concentrations below uncertainty are determined to have no signal, and, for concentrations above uncertainty, the difference between concentration (x_i) and uncertainty (s_i) is used as the signal:

$$d_{ij} = \left(\frac{x_{ij} - s_{ij}}{s_{ij}} \right) \quad \text{if } x_{ij} > s_{ij}$$

$$d_{ij} = 0 \qquad \text{if } x_{ij} \le s_{ij}$$

S/N is then calculated using Equation A1.6:

$$\left(\frac{S}{N} \right)_j = 1/n \sum_{i=1}^{n} d_{ij} \qquad \text{Equation A1.6}$$

The result with this S/N calculation is that species with concentrations always below their uncertainty have a S/N of 0. Species with concentrations that are twice the uncertainty value have a S/N of 1. S/N greater than 1 may often indicate a species with a 'good' signal, although this depends on how uncertainties were determined. Negative concentration values do not contribute to the S/N, and species with a handful of high-concentration events will not have artificially high S/N (Norris et al. 2014).

Species category: This enables the user to specify whether the elemental species should be considered:

- Strong – whereby the element is generally present in concentrations well above the limit of detection (high S/N) and the uncertainty matrix is a reasonable representation of the errors.
- Weak – where the element may be present in concentrations near the limit of detection (low S/N), where there is doubt about some of the measurements and/or the error estimates or where the elemental species is only detected some of the time. If 'Weak' is chosen, EPAPMF increases the user-provided uncertainties for that variable by a factor of 3.
- Bad – that variable is excluded from the model run.

For this work, an element with concentrations at least three times above the limit of detection, a high S/N (>2) and that was present in all samples was generally considered 'Strong'. Variables were labelled as 'Weak' if their concentrations were generally low, had a low S/N, were only present in a few samples or if there was a lower level of confidence in their measurement. Mass concentration gravimetric measurements and black carbon were also down-weighted as 'Weak' depending on the dataset because their concentrations are generally several orders of magnitude above other species, which can have the tendency to 'pull' the model. Paatero and Hopke (2003) recommend that such variables be down-weighted and that it does not particularly affect the model fitting if those variables are from real sources – what does affect the model severely is if a dubious variable is over-weighted. Elements that had a low S/N (<0.5) were examined using bi-variate correlation plots to determine inter-species relationships. Those low S/N variables with little or no association with other species, or that had mostly zero values, or were doubtful for any reason, were labelled as 'Bad' and were subsequently not included in the analyses.

If the model is appropriate for the data and if the uncertainties specified are truly reflective of the uncertainties in the data, then Q (according to Eberly [2005]) should be approximately equal to the number of data points in the concentration dataset:

$$Theoretical\ Q = \#\ samples \times \#\ species\ measured \qquad \text{Equation A1.7}$$

However, a slightly different approach to calculating the Theoretical Q value was recommended by Brown and Hafner (2005), which takes into account the degrees of freedom in the PMF model and the additional constraints in place for each model run. This theoretical Q calculation Q_{th} is given as:

$$Q_{th} = (\#\ samples \times \#\ good\ species) + [(\#\ samples \times \#\ weak\ species)/3] - (\#\ samples \times factors\ estimated) \qquad \text{Equation A1.8}$$

Both approaches have been taken into account for this study, and it is likely that the actual value lies somewhere between the two. Further guidance has more recently been provided by Paatero et al. (2014) and Brown et al. (2015), where a third parameter, $Q_{expected}$, should also be calculated, but only the 'good' or non-weak variables should be taken into account:

$$\textit{The expected value of Q is approximately} = \textit{(number of non-weak data values in X)} - \textit{(numbers of elements in G and F, taken together)} \quad \text{Equation A1.9}$$

A down-weighted weak variable has only a small, rarely significant, contribution to $Q_{expected}$ and, for simplicity, is excluded here. If the Q value of the chosen model differs significantly from what is expected (e.g. by a factor of 10 or more), then DISP error analysis becomes invalid and BS-DISP is likely questionable.

In PMF, it is assumed that only the x_{ij} values are known and that the goal is to estimate the contributions (g_{ik}) and the factors (or profiles) (f_{kj}). It is assumed that the contributions and mass fractions are all non-negative, hence the 'constrained' part of the least squares. Additionally, EPAPMF allows the user to say how much uncertainty there is in each x_{ij}. Species-days with lots of uncertainty are not allowed to influence the estimation of the contributions and profiles as much as those with small uncertainty, hence the 'weighted' part of the least squares and the advantage of this approach over PCA.

Diagnostic outputs from the PMF models were used to guide the appropriateness of the number of factors generated and how well the receptor modelling was accounting for the input data. Where necessary, initial solutions have been 'rotated' to provide a better separation of factors (sources) that were considered physically reasonable (Paatero et al. 2002). Each PMF model run reported in this study is accompanied by the modelling statistics, along with comments where appropriate.

A1.8 Dataset Quality Assurance

Quality assurance of sample elemental datasets is vital so that any dubious samples, measurements and outliers are removed, as these will invariably affect the results of receptor modelling. In general, the larger the dataset used for receptor modelling, the more robust the analysis. The following sections describe the methodology used to check data integrity and provide a quality-assurance process that ensured that the data being used in subsequent factor analysis was as robust as possible.

A1.8.1 Mass Reconstruction and Mass Closure

Once the sample analysis for the range of analytes has been carried out, it is important to check that total measured mass does not exceed gravimetric mass (Cohen 1999). Ideally, when elemental analysis and organic compound analysis has been undertaken on the same sample, one can reconstruct the mass using the following general equation for ambient samples as a first approximation (Cahill et al. 1989; Malm et al. 1994; Cohen 1999):

$$\textit{Reconstructed mass} = \textit{[Soil]} + \textit{[OC]} + \textit{[BC]} + \textit{[Smoke]} + \textit{[Sulphate]} + \textit{[Sea salt]} \quad \text{Equation A1.10}$$

where:

- *[Soil]* = 2.20[Al] + 2.49[Si] + 1.63[Ca] + 2.42[Fe] + 1.94[Ti]
- *[OC]* = Σ[Concentrations of organic compounds]
- *[BC]* = Concentration of black carbon (soot)

- *[Smoke]* = [K] − 0.6[Fe]
- *[Sea salt]* = 2.54[Na]
- *[Sulphate]* = 4.125[S]

The reconstructed mass is based on the fact that the six composite variables or 'pseudo' sources given in Equation A1.10 are generally the major contributors to fine- and coarse-particle mass and are based on geochemical principles and constraints. The *[Soil]* factor contains elements predominantly found in crustal matter (Al, Si, Ca, Fe, Ti) and includes a multiplier to correct for oxygen content and an additional multiplier of 1.16 to correct for the fact that three major oxide contributors (MgO, K_2O, Na_2O), carbonate and bound water are excluded from the equation.

[BC] is the concentration of black carbon, measured in this case by light reflectance/ absorbance. *[Smoke]* represents K not included as part of crustal matter and tends to be an indicator of biomass burning.

[Sea salt] represents the marine aerosol contribution and assumes that the NaCl weight is 2.54 times the Na concentration. Na is used, as it is well known that chlorine can be volatilised from aerosol or from filters in the presence of acidic aerosol, particularly in the fine fraction via the following reactions (Lee et al. 1999):

$$NaCl(p) + HNO_3(ag) \rightarrow NaNO_3(p) + HCL(g) \quad \text{Equation A1.11}$$

$$2NaCl(p) + H_2SO_4(ag) \rightarrow Na_2SO_4(p) + 2HCL(g) \quad \text{Equation A1.12}$$

Alternatively, where chlorine loss is likely to be minimal, such as in the coarse fraction or for both size fractions near coastal locations and relatively clean air in the absence of acid aerosol, then the reciprocal calculation of *[Sea salt] = 1.65[Cl]* can be substituted, particularly where Na concentrations are uncertain.

Most fine sulphate particles are the result of oxidation of SO_2 gas to sulphate particles in the atmosphere (Malm et al. 1994). It is assumed that sulphate is present in fully neutralised form as ammonium sulphate. *[Sulphate]* therefore represents the ammonium sulphate contribution to aerosol mass with the multiplicative factor of 4.125[S] to account for ammonium ion and oxygen mass (i.e. $(NH_4)_2SO_4$ = *[(14 + 4)2 + 32 + (16 x 4)/32]*).

Additionally, the sulphate component not associated with sea salt can be calculated from Equation A1.13 (Cohen 1999):

$$\text{Non-sea salt sulphate (NSS-Sulphate)} = 4.125\,([S_{tot}] - 0.0543[Cl]) \quad \text{Equation A1.13}$$

where the sulphur concentrations contributed by sea salt are inferred from the chlorine concentrations, i.e. [S/Cl] sea salt = 0.0543 and the factor of 4.125 assumes that the sulphate has been fully neutralised and is generally present as $(NH_4)_2SO_4$ (Cahill et al. 1989; Malm et al. 1994; Cohen 1999).

The reconstructed-mass and mass-closure calculations using the pseudo-source and pseudo-element approach are a useful way to examine initial relationships in the data and how the measured mass of species in samples compares to gravimetric mass. Note that some scatter is possible because not all aerosols are necessarily measured and accounted for, such as all organic compounds, ammonium species, nitrates and unbound water.

A1.8.2 Dataset Preparation

Careful preparation of a dataset is required because serious errors in data analysis and receptor-modelling results can be caused by erroneous individual data values. The general methodology followed for dataset preparation was as recommended by Brown and Hafner (2005) and the EPAPMF 5.0 User Guide (Norris et al. 2014). For this study, all data were checked for consistency with the following parameters:

- Individual sample collection validation.
- Gravimetric mass validation.
- Analysis of reconstructed mass versus gravimetric mass to assess mass closure and linearity.
- Identification of unusual values, including noticeably extreme values and values that normally track with other species (e.g. Al and Si) but deviate in one or two samples. Scatter plots and time-series plots were used to identify unusual values. One-off events such as fireworks displays, forest fires or vegetative burn-offs may affect a receptor model, as it is forced to find a profile that matches only that day.
- Species were included in a dataset if at least 70% of data was above the limit of detection and signal-to-noise ratios were checked to ensure that data had sufficient variability. Important tracers of a source where less than 70% of data were above the limit of detection were included, but model runs with and without the data were used to assess the effect.

In practise, during data analyses, the above steps were a re-iterative process of cross-checking as issues were identified and corrected for, or certain data excluded, and the effects of this were then studied.

A1.8.2.1 Positive Matrix Factorisation Data Matrix Population

The following steps were followed to produce a final dataset for use in the PMF receptor model (Brown and Hafner 2005).

- **Below-detection-limit data:** For given values, the reported concentration used and corresponding uncertainty was checked to ensure that it had a high value.
- **Missing data:** Substituted with the dataset median value for that species.

A1.8.2.2 Positive Matrix Factorisation Uncertainty Matrix Population

Uncertainties can have a large effect on model results, so these must be carefully compiled. The effect of under-estimating uncertainties can be severe, while over-estimating uncertainties does not do too much harm (Paatero and Hopke 2003).

- **Uncertainties for data:** Uncertainties for the IBA elemental data were calculated using the following equations (Kara et al. 2015):
  - $\sigma_{ij} = x_{ij} + 2/3(DL_j)$ for samples below limit of detection; and
  - $\sigma_{ij} = 0.2x_{ij} + 2/3(DLj)$; $DL_j < x_{ij} < 3DL_j$ and $\sigma_{ij} = 0.1x_{ij} + 2/3(DL_j)$; $x_{ij} > 3DL_j$: for detected values

  where x_{ij} is the determined concentration for species j in the i^{th} sample and DL_j is the detection limit for species j.

- **Missing data:** Uncertainty was calculated as 4 × median value over the entire species dataset.
- **PM gravimetric mass:** Uncertainty given as 4 × mass value to down-weight the variable.

Re-iterative model runs were used to examine the effect of including species with high uncertainties or low concentrations. In general, it was found that the initial uncertainty estimations were sufficient and that adjusting the 'additional modelling uncertainty' function accommodated any issues with modelled variables, such as those with residuals outside ± 3 standard deviations.

APPENDIX 2 HASTINGS DATA-ANALYSIS SUMMARY

Using the methodology outlined in Section A1.4.1, Figure A2.1 presents the mass reconstruction results for Hastings $PM_{2.5}$ and PM_{10}. Figure A2.2 presents a correlation matrix plot for key elemental species in the two size fractions.

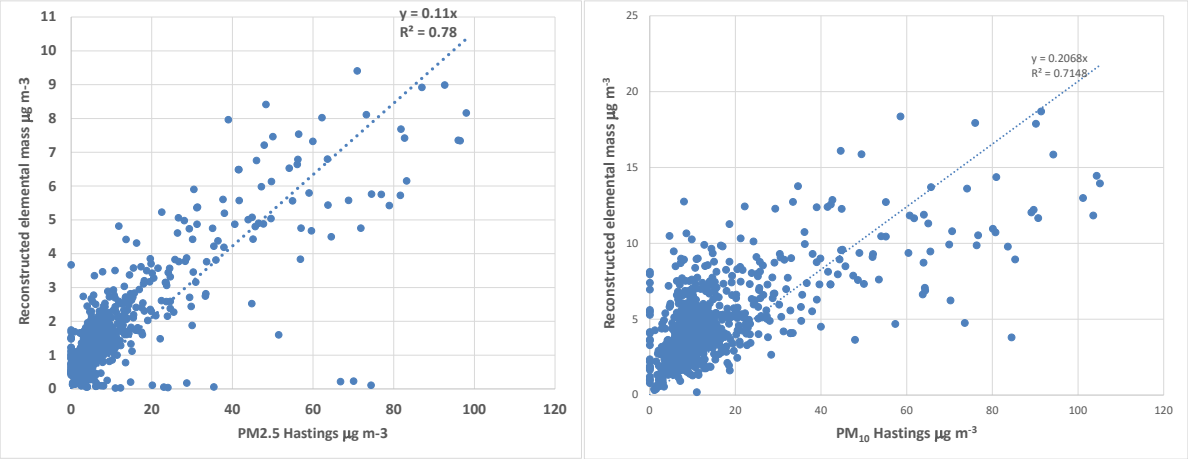

Figure A2.1 Plot of Hastings $PM_{2.5}$ (left) and PM_{10} (right) elemental mass reconstruction against gravimetric mass.

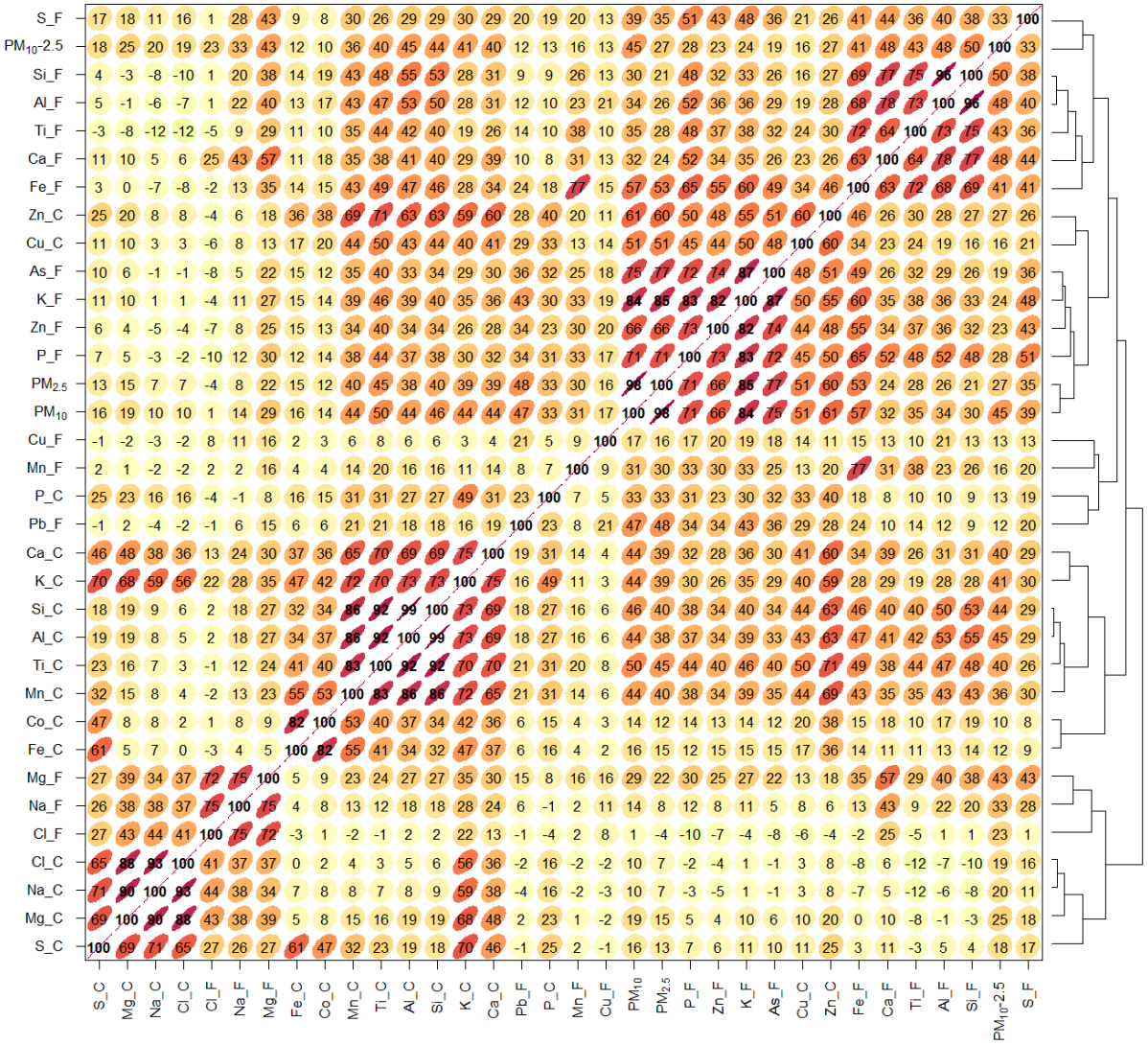

Figure A2.2 Particulate matter and key elemental composition correlation plot for Hastings $PM_{2.5}$ and PM_{10} samples.

A2.1 Hastings Positive Matrix Factorisation Receptor-Modelling Diagnostics

PMF analyses involve many details about the development of the data, decisions of what data to include/exclude, determination of a solution and evaluation of robustness of that solution. The following diagnostics for the PMF solutions are reported as recommended by Paatero et al. (2014) and Brown et al. (2015) and should be read in conjunction with Section 2.1 and Appendix 1. A critical factor in the success of receptor modelling is the ability to reproduce observed versus predicted (modelled) mass. This was achieved to an acceptable level in the case of Hastings $PM_{2.5}$ and PM_{10}, as presented in Figure A2.3.

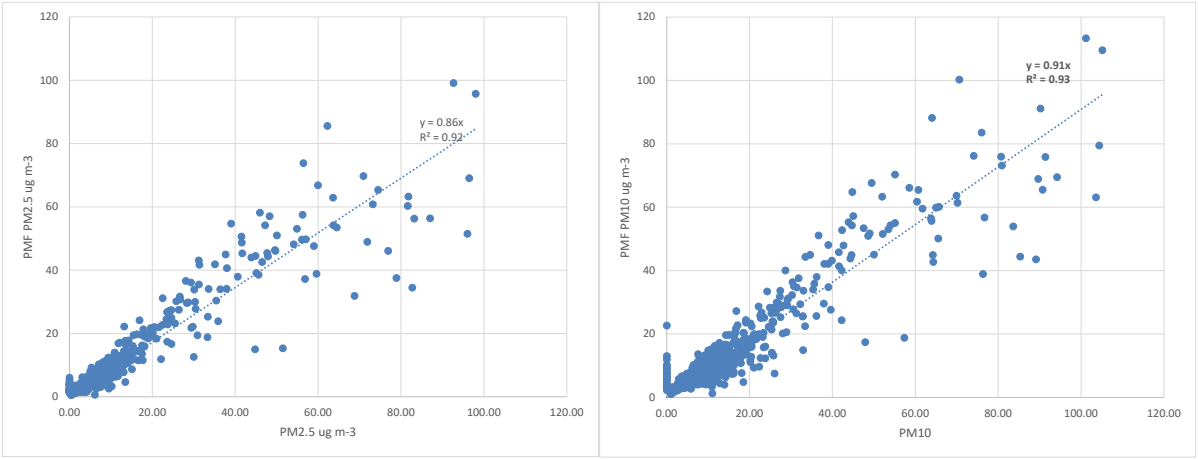

Figure A2.3 Plot of Hastings $PM_{2.5}$ (left) and PM_{10} (right) predicted (PMF) mass against observed gravimetric mass.

Table A2.1 Summary of EPAPMF settings for receptor modelling of Hastings $PM_{2.5}$. and PM_{10}.

Parameter	Setting
Data type; averaging timeframe	12-hour
N samples	836
N factors	5
Treatment of missing data	No missing data
Treatment of data below detection limit (BDL)	Data used as reported, no modification or censoring of BDL data
Lower limit for normalised factor contributions gik	-0.2
Robust mode	Yes
Constraints	None
Seed value	Random
N bootstraps in BS	200
r^2 for BS	0.6
DISP dQmax	4, 8, 16, 32
DISP active species	$PM_{2.5}$, BC, Al_F, Si_F, S_F, Cl_F, K_F, Ca_F, Fe_F, Zn_F, As_F, Na_Gam_C, Mg_C, Al_C, Si_C, S_C, Cl_C, K_C, Ca_C, Ti_C, Fe_C, Cu_C, Zn_C, Na_Gam_PM10, Mg_PM10, Al_PM10, Si_PM10, S_PM10, Cl_PM10, K_PM10, Ca_PM10, Ti_PM10, Mn_PM10, Fe_PM10, Cu_PM10, Zn_PM10, As_PM10
N bootstraps; r^2 for BS in BS-DISP	200; 0.6
BS-DISP active species	BC, Al_F, Si_F, S_F, Cl_F, K_F, Ca_F, Fe_F, Zn_F, As_F, Na_Gam_C, Mg_C, Al_C, Si_C, S_C, Cl_C, K_C, Ca_C, Ti_C, Fe_C, Cu_C, Zn_C, Na_Gam_PM10, Mg_PM10, Al_PM10, Si_PM10, S_PM10, Cl_PM10, K_PM10, Ca_PM10, Ti_PM10, Mn_PM10, Fe_PM10, Cu_PM10, Zn_PM10, As_PM10
BS-DISP dQmax	0.5, 1, 2, 4
Extra modelling uncertainty	15%

Table A2.2 Output diagnostics for receptor modelling of Hastings $PM_{2.5}$.

Diagnostic	Four Factors
$Q_{Theoretical}$	17514
$Q_{Expected}$	15664
Q_{true}	12043
Q_{robust}	12043
$Q_{robust}/Q_{expected}$	0.496
DISP Diagnostics	
Error code	0
Largest decrease in Q	0
DISP % dQ	0
DISP swaps by factor	0
BS-DISP Diagnostics	
BS mapping (Fpeak BS) – unmapped	99% (100%) – 0
BS-DISP % cases accepted	99%
Largest decrease in Q	-0.274
BS-DISP % dQ	-0.0023
No. of decreases in Q	0
No. of swaps in best fit	2
No. of swaps in DISP	0
BS-DISP swaps by factor	0, 0, 0, 0,2

www.gns.cri.nz

Principal Location

1 Fairway Drive, Avalon
Lower Hutt 5010
PO Box 30368
Lower Hutt 5040
New Zealand
T +64-4-570 1444
F +64-4-570 4600

Other Locations

Dunedin Research Centre
764 Cumberland Street
Private Bag 1930
Dunedin 9054
New Zealand
T +64-3-477 4050
F +64-3-477 5232

Wairakei Research Centre
114 Karetoto Road
Private Bag 2000
Taupo 3352
New Zealand
T +64-7-374 8211
F +64-7-374 8199

National Isotope Centre
30 Gracefield Road
PO Box 30368
Lower Hutt 5040
New Zealand
T +64-4-570 1444
F +64-4-570 4657